Diversification of mammalian deltaviruses by host shifting

Laura M. Bergner[1,2*], Richard J. Orton[2], Alice Broos[2], Carlos Tello[3,4], Daniel J. Becker[5–7], Jorge E. Carrera[8–9], Arvind H. Patel[2], Roman Biek[1], Daniel G. Streicker[1,2]

[1] Institute of Biodiversity, Animal Health and Comparative Medicine, College of Medical, Veterinary and Life Sciences, University of Glasgow, Glasgow, United Kingdom

[2] MRC–University of Glasgow Centre for Virus Research, Glasgow, United Kingdom

[3] Association for the Conservation and Development of Natural Resources, Lima, Perú

[4] Yunkawasi, Lima, Perú

[5] Odum School of Ecology, University of Georgia, Athens, USA

[6] Center for the Ecology of Infectious Diseases, University of Georgia, Athens, USA

[7] Department of Biology, Indiana University, Bloomington, USA

[8] Departamento de Mastozoología, Museo de Historia Natural, Universidad Nacional Mayor de San Marcos, Lima, Perú

[9] Programa de Conservación de Murciélagos de Perú, Piura, Perú

*Corresponding author: Laura Bergner (Laura.Bergner@glasgow.ac.uk)

Abstract

Hepatitis deltavirus (HDV) is an obligate hyper-parasite that increases the severity of hepatitis B virus (HBV) in humans. The origins of HDV and the mechanisms through which it and related animal deltaviruses diversify are unknown. We report the epidemiology and evolutionary history of new mammal-infecting deltaviruses. Despite geographic under-representation in over 348 terabases of globally-distributed RNA sequence data from mammals, deltaviruses originated exclusively from the Americas, infecting bats, rodents and a cervid. Phylogenetic analyses revealed multiple host shifts among mammalian orders. Consistent absence of HBV-like viruses in two deltavirus-infected bat species indicated acquisitions of novel helper viruses during the divergence of animal and human-infecting deltaviruses. Our analyses support an American zoonotic origin of HDV and show that deltaviruses can diversify by host shifting despite dependence on unrelated viruses.

Main Text

Hepatitis delta virus (HDV) is a globally-distributed human pathogen which causes the most severe form of viral hepatitis in an estimated 20 million people. Unlike typical viruses, HDV is an obligate 'satellite' virus that is replicated by diverse host cells, but requires the envelope of an unrelated 'helper' virus (classically hepatitis B virus, HBV, family *Hepadnaviridae*) for cellular entry, egress and transmission (*1*). The peculiar life history of HDV together with its lack of sequence homology to known viral groups has made the evolutionary origins of HDV a longstanding puzzle. Geographic associations of most HDV genotypes point to an Old World origin. Yet, historical explanations of the mechanistic origin of HDV spanned from emergence from the mRNA of a HBV-infected human (*2*) to ancient evolution from viroids (circular, single-stranded RNA pathogens of plants) (*3*). More recently, discoveries of HDV-like genomes in vertebrates and invertebrates (*4-7*) overturned the decades-long belief that deltaviruses exclusively infect humans. These discoveries also suggested new models of deltavirus evolution, in which viruses either co-speciated with their hosts over ancient timescales or possess an unrecognized capacity for host shifting which would imply their potential to emerge in novel species.

Efforts to distinguish competing evolutionary hypotheses for deltaviruses have been precluded by the remarkably sparse distribution of currently-known HDV-like agents across the animal tree of life. Single representatives are reported from arthropods (Subterranean termite, *Schedorhinotermes intermedius*), fish (a pooled sample from multiple species), birds (a pooled sample from 3 duck species, *Anas gracilis*, *A. castanea*, *A. superciliosa*), reptiles (Common boa, *Boa constrictor*) and mammals (Tome's spiny rat, *Proechimys semispinosus*), and only two are known from amphibians (Asiatic toad, *Bufo gargarizans*; Chinese fire belly newt, *Cynops orientalis*) (*4-7*). Most share minimal homology with HDV, even at the protein level (< 25%), frustrating robust phylogenetic re-constructions of evolutionary histories (Fig. S1). On the one hand, the distribution of deltaviruses may reflect rare host shifting events among divergent taxa. Alternatively, reliance on untargeted metagenomic sequencing (a relatively new and selectively applied tool) to find novel species may mean that the distribution of deltaviruses in nature is largely incomplete (*8*, *9*). Additional taxa could reveal ancient co-speciation of HDV-like agents with their hosts or evidence for host shifting.

We sought to fill gaps in the evolutionary history of mammalian deltaviruses, the group most likely to clarify the origins of HDV. We used a two-pronged approach (Materials and Methods). First, we used data from Serratus, a newly developed bioinformatic platform which screens RNA sequences from the NCBI Short Read Archive (SRA) for similarity to known viruses and which is described by Edgar *et al.* (*10*). We focused on search results from 96,695 transcriptomic and metagenomic datasets, comprising 348 terabases of RNA sequences from 403 species across 24 mammalian orders (22 terrestrial, 2 aquatic; Data S1). Although domesticated animals comprised the largest single fraction of the dataset (67.2%), remaining data were from a variety of globally-distributed species (Fig 1A,B). Our second search was prompted by our earlier detection of uncharacterized deltavirus-like sequences in a neotropical bat (*11*) and evidence of under-representation in the volume of neotropical bat data in the SRA (Fig. 1A). We therefore carried out metagenomic sequencing of 23 frugivorous, insectivorous, nectarivorous, and sanguivorous bat species from Peru, using 59 samples available within our laboratory (Table S1). All datasets containing sequences with significant protein homology to deltaviruses were subjected to *de novo* genome assembly.

Searches revealed five deltaviruses spanning three mammalian orders: Artiodactyla (N=1), Chiroptera (N=3), and Rodentia (N=1; Fig. 1C). Strikingly, despite over-representation of Old World-derived data by factors of 4.3 (Artiodactyla), 5.8 (Chiroptera), 2.1 (Rodentia), all new mammalian deltaviruses originated from North and South American species (Supplementary Results Section 1, Fig. 1A,C). Chiropteran deltaviruses included two genotypes from common vampire bats (*Desmodus rotundus*) which shared only 48.4-48.6% genome-wide nucleotide (nt) identity (hereafter, DrDV-A and DrDV-B; Fig. S1). A third deltavirus was identified in a liver transcriptome (accession SRR7910143; (*12*)) from a lesser dog-like bat (*Peropteryx macrotis*) from Mexico (PmacDV), but was more closely related to recently described deltaviruses from Tome's spiny rat from Panama (PsemDV; (*7*)), sharing 95.9-97.4% (amino acid) and 93.0-95.7% (nt) identity. Additional genomes were recovered from transcriptomes derived from the pedicle tissue of a white-tailed deer (*Odocoileus virginianus*; OvirDV; accession SRR4256033; (*13*)) and from a captive-born Eastern woodchuck (*Marmota monax*; MmonDV; accession SRR2136906; (*14*)). Bioinformatic screens recovered additional reads matching each genome in related datasets (either different individuals from the same study or different tissues from the same individuals), suggesting active infections (Table S2). All genomes had lengths 1669-1771

nucleotides, high intramolecular base pairing, and contained genomic and antigenomic ribozymes characteristic of deltaviruses. The DrDV-A and DrDV-B genomes are more fully characterized in Fig S2, Fig S3, Table S3 and Supplementary Results Section 2. The other genomes and a case study on MmonDV infections in animals inoculated with woodchuck hepatitis virus are described by Edgar *et al.* (*10*).

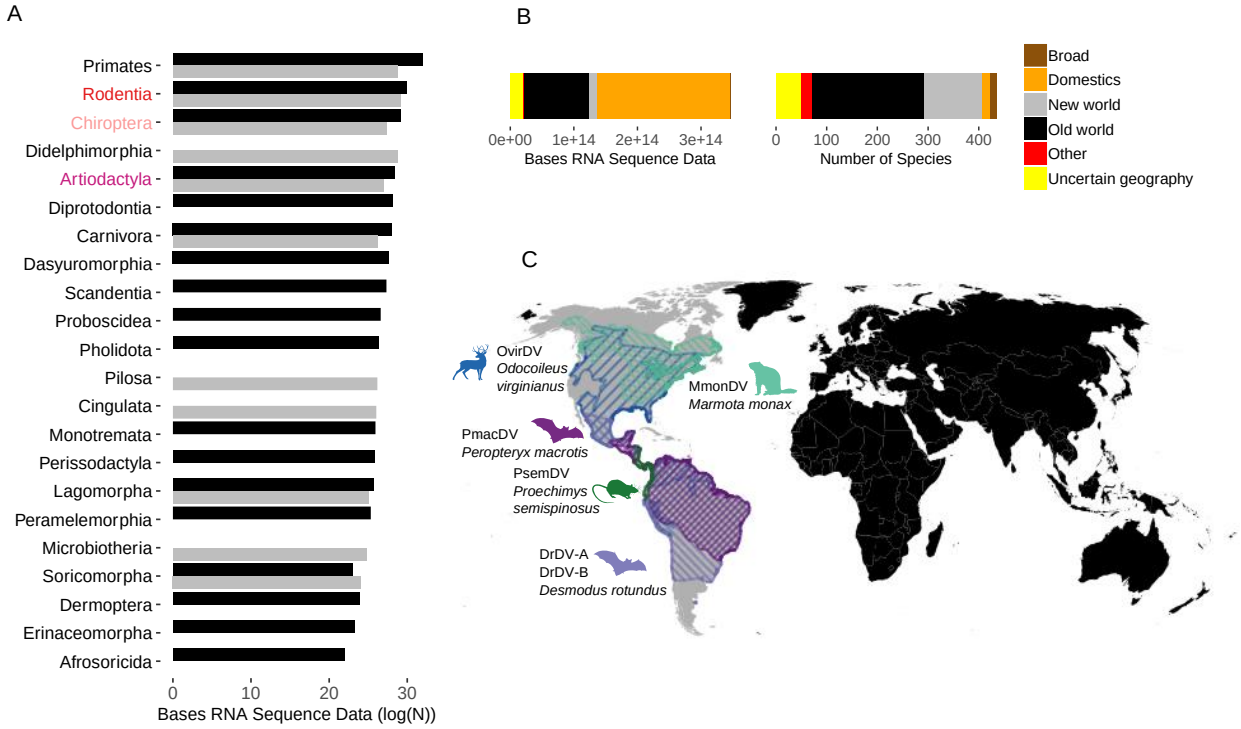

Fig. 1. Geographic and taxonomic distribution of mammalian datasets and novel deltaviruses. (**A**) The host and geographic distribution of metagenomic and transcriptomic datasets searched for novel deltaviruses, note the log scale. Colors indicate orders (red = Rodentia; pink = Chiroptera; Purple = Artiodactyla). (**B**) Stacked bar charts show the volume of mammalian datasets in units of RNA bases and the number of species searched, separated by species geography. Additional segments describe widely distributed domesticated animals (Domestics), datasets with genus-level metadata from broadly-distributed genera (Broad), datasets from cell lines or with taxonomic information only at the Class level (Other), and those which had no geographic range data available (Uncertain geography, mostly aquatic mammals). (**C**) Host distributions of newly discovered and recently reported deltaviruses, color coded by mammalian species (Data from IUCN). All except PsemDV were discovered through our search.

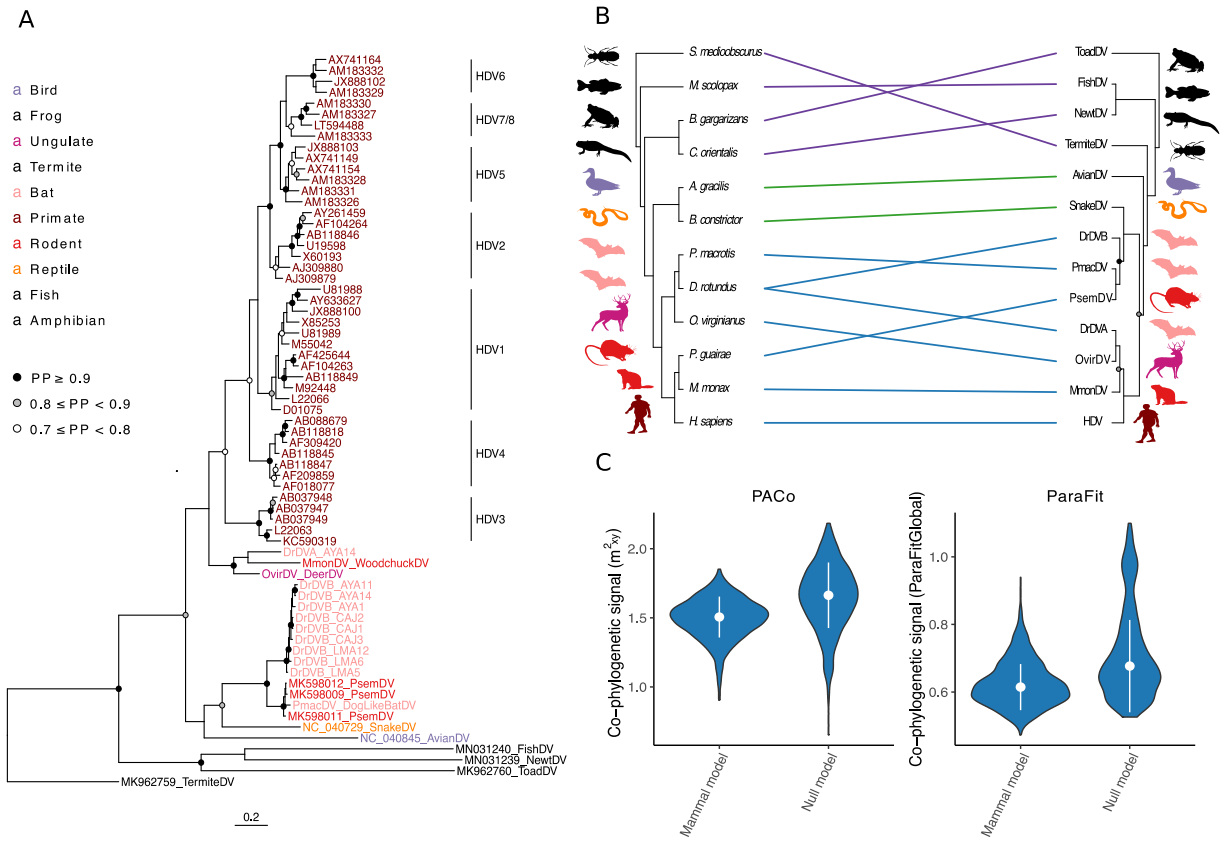

Fig. 2. Evolutionary history of deltaviruses reveals host shifts among mammals. (**A**) Bayesian phylogeny of a 192 amino acid alignment of the DAg. Ingroup taxa including mammal, snake and avian deltaviruses are colored by order; other HDV-like taxa are shown in black. (**B**) Co-phylogeny depicting connections between the consensus deltavirus phylogeny from StarBeast and the host tree (from TimeTree.org). Links are colored according to subsets of data used in co-phylogenetic analyses; all taxa (purple + green + blue), ingroup (green + blue), or mammal (blue). Host taxa are: *Schedorhinotermes medioobscurus*, *Macroramphosus scolopax*, *Bufo gargarizans*, *Cynops orientalis*, *Anas gracilis*, *Boa constrictor*, *Peropteryx macrotis*, *Desmodus rotundus*, *Odocoileus virginianus*, *Proechimys guirae*, *Marmota monax*, and *Homo sapiens*. (**C**) Absence of phylogenetic dependence of the mammalian deltavirus phylogeny on the host phylogeny. Violin plots show distributions of test statistics from two co-phylogenetic approaches across 1,000 posterior trees relative to null models, along with medians and standard deviations. For PACo, higher values would indicate greater phylogenetic dependence; for ParaFit, lower values. Both approaches rejected a global model of co-speciation ($P > 0.05$).

Phylogenetic analysis of the small delta antigen (DAg) protein sequences using MrBayes (Fig. 2A) and a multi-species coalescent model in StarBeast (Fig. 2B) revealed multiple putative host shifts within the evolutionary history of mammalian deltaviruses. For instance, vampire bat deltaviruses were paraphyletic, suggesting at least two independent incursions into this species. Specifically, DrDV-A formed a clade with OvirDV and MmonDV (posterior probability, *PP* =

0.99/0.80 in MrBayes and StarBeast respectively) which was basal to HDV (*PP* = 0.65/0.81), while DrDV-B shared a most recent common ancestor with PmacDV and PsemDV (*PP* = 1/1). Rodent-associated deltaviruses (MmonDV and PsemDV) were also highly divergent and paraphyletic. Consequently, co-phylogenetic analyses using 1,000 randomly sampled topologies from StarBeast failed to reject independence of mammal and deltavirus phylogenies, consistent with a model of diversification by host shifting (Fig. 2B,C). Analyses of all deltavirus-host pairs (i.e. including highly divergent HDV-like agents) and an 'ingroup' clade containing mammalian along with avian and snake deltaviruses revealed somewhat greater dependence of the deltavirus phylogeny on the host phylogeny (Fig. S4). However, statistical significance varied across co-phylogenetic approaches and topological incongruences were evident among non-mammals, excluding co-speciation as the sole diversification process, even in deeper parts of the co-evolutionary history (Fig. S5, Supplementary Results Section 3).

Having extended the mammalian host range of deltaviruses to neotropical bats, we subsequently explored the transmission dynamics, host range, and candidate helper virus associations within this group through a field study in three regions of Peru (Fig. 3A). Out of 240 *D. rotundus* saliva samples from 12 bat colonies collected in 2016-2017, RT-PCR targeting the DAg detected DrDV-A in single adult female from one of the two metagenomic pools that contained this genotype (bat ID 8299, site AYA14, Table S4, S5). In contrast, DrDV-B was detected in 17.1% of *D. rotundus* saliva samples (colony-level prevalence: 0-35%). Prevalence varied neither by region of Peru (Likelihood ratio test; $\chi^2 = 3.21$; d.f. = 2; $P = 0.2$) nor by bat age or sex (binomial generalized linear mixed model, Age: $P = 0.38$; Sex: $P = 0.87$), suggesting geographic and demographic ubiquity of infections. Given that vampire bats subsist on blood, deltavirus sequences encountered in bat saliva might represent contamination from infected prey. A small set of blood samples screened for DrDV-A (N = 60, including bat 8299) were negative. However, 6 out of 41 bats that were DrDV-B negative and 4 out of 18 bats with DrDV-B in saliva also contained DrDV-B in blood samples (Fig. 3B). In the 4 individuals with paired saliva and blood samples, DAg sequences were identical, supporting systemic infections. Significant spatial clustering of DrDV-B sequences at both regional and bat colony levels further supported local infection cycles driven by horizontal transmission among vampire bats (Fig. 3A; Table S6).

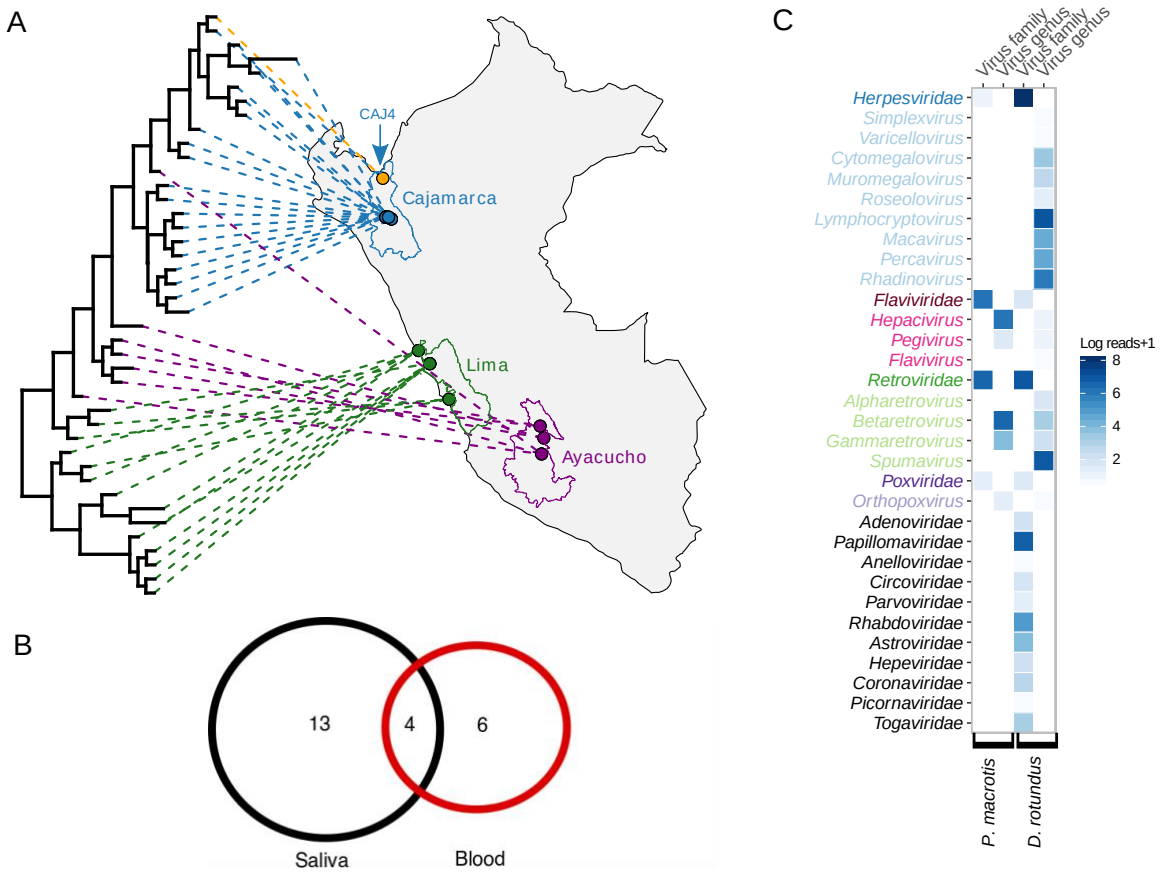

Fig. 3. Transmission biology and candidate helper viruses for bat deltaviruses. (**A**) Bayesian phylogeny of a 214 nt alignment of DrDV-B DAg projected onto vampire bat capture locations in Peru. Lines and points are colored by administrative regions. Site CAJ4, where the *C. perspicillata* sequence was detected, is depicted in orange. (**B**) DrDV-B detections in saliva and blood. Numbers represent individual bats; the four bats in the center had genetically identical DrDV-B sequences in saliva and blood. (**C**) Mammal-infecting viral communities are shown for the *P. macrotis* liver transcriptome which contained PmacDV and combined *D. rotundus* saliva metagenomes. Viral taxa are colored by family, with lighter shades indicating genera within families, for overlapping viral families in both bat species. Viral families only present in one bat species are shown in black. Candidate helpers for OvirDV and MonDV are shown in Fig. S8.

Given the evolutionary evidence for deltavirus host shifts, we hypothesized that spillover infections might also occur at detectable frequencies in sympatric neotropical bats. Among 87 non-*D. rotundus* bats captured in or outside of *D. rotundus*-occupied roosts, RT-PCR detected deltavirus RNA in the saliva of a single Seba's short-tailed bat (*Carollia perspicillata;* N=31 individuals; Fig. S6). This result was unlikely attributable to erroneous bat species assignment or laboratory contamination (Supplementary Results, Section 4). The partial DAg recovered from

the *C. perspicillata* was identical to a DrDV-B strain collected from a vampire bat in the same roost (CAJ4; Fig. 3A). Given the rapid evolution expected in deltaviruses (ca. 10^{-3} substitutions/site/year), genetic identity is most parsimoniously explained as horizontal transmission from *D. rotundus* to *C. perspicillata*, which was followed by an absence of (or short-lived) transmission among *C. perspicillata* at the time of sampling (*15*). This finding therefore demonstrates cross-species transmission on ecological timescales, a defining prerequisite for evolutionary diversification of deltaviruses through host shifting.

Finally, we evaluated whether bat deltaviruses use hepadnavirus helpers akin to HDV (*1*). Consistent with a previous study, PCR screens of DrDV-positive and negative saliva (N=54) and blood samples (N=119), found no evidence of hepadnaviruses in vampire bats (*16*). To rule out divergent hepadnaviruses missed by PCR, we next used a bioinformatic pipeline to characterize viral communities in the metagenomic and transcriptomic datasets from deltavirus-infected bat species (Materials and Methods). Hepadnaviruses were again absent from all datasets (Fig. 3C). Together with the finding that all three bat-infecting deltavirus genomes lacked the farnesylation site thought to facilitate acquisition of the hepadnaviral envelope (Supplementary Results, Section 2), use of hepadnavirus helpers by bat deltaviruses seems unlikely. To identify alternative plausible candidates, we quantified the abundance (approximated by sequence reads) of viral taxa that overlapped between the two deltavirus-infected bat species, *P. macrotus* and *D. rotundus*. In the *P. macrotus* liver which contained PMacDV, reads from hepaciviruses (*Flaviviridae*) spanned a complete viral genome and outnumbered all other viral genera with the exception of Betaretroviruses, whose abundance reflects endogenization in the host genome (Fig. 3C). Lower, but detectable, hepacivirus abundance in vampire bats may reflect the tissue tropism of these viruses or pooling of samples from multiple individuals. Intriguingly, hepaciviruses experimentally mobilize HDV *in vitro* and were found in 26 out of 30 PsemDV-infected rats (*7*, *17*). Reads matching Poxviridae formed small contigs in both libraries (*P. macrotus*: 229-1386 nt; *D. rotundus*: 358 nt) and particularly in *D. rotundus*, could not be excluded as false positives. Although non-opportunistic sampling is required to decisively identify the helpers of bat deltaviruses, existing evidence points to hepaciviruses as top contenders, perhaps using alternative enveloping mechanisms to HDV.

Unlike conventional pathogens (e.g., viruses, bacteria, protozoans), the obligatory dependence of deltaviruses on evolutionarily independent helpers creates a barrier to cross-

species transmission that might be expected to promote host specificity. Data to test this hypothesis have been unavailable until now. Our study demonstrates transmission of deltaviruses among highly divergent mammalian orders on both ecological and evolutionary timescales.

Deltavirus host shifts could conceivably arise through several processes. Mobilization by non-viral micro-organisms (e.g., intra-cellular bacteria) is conceivable but has never been observed. Unaided spread through a yet undefined mechanism is also possible. However, given that the best-studied deltavirus (HDV) depends on viral envelopes to complete its life cycle and that conserved genomic features in related deltaviruses suggest a similar life history strategy, helper virus mediated host shifting is the most reasonable expectation. We and others have excluded hepadnavirus helpers for PmacDV, DrDVs, and PsemDV, yet natural HDV infections consistently involve HBV (*1*, *7*). In light of this and the evidence presented here for host shifts among mammals, the contemporary HDV-HBV association must have arisen through acquisition of the hepadnaviral helper somewhere along the evolutionary divergence separating human and other mammal-infecting deltaviruses. Evidence that deltaviruses can exploit diverse enveloped viruses experimentally adds further weight to this conclusion (*17*, *18*). As several new mammalian deltaviruses were detected with hepacivirus and poxvirus co-infections, either simultaneous host shifts of deltaviruses and helpers, or preferential deltavirus shifting among host species that are already infected with compatible helpers are plausible. Conclusively identifying the helper associations of novel mammalian deltaviruses and their evolutionary relationships will be crucial to disentangling these possibilities.

A limitation of our study was that the species in which novel deltaviruses were discovered were presumed to be definitive hosts (i.e. capable of sustained horizontal transmission). Consequently, some putative host shifts detected in our co-phylogenetic analysis may represent short-lived transmission chains in novel hosts or singleton infections, analogous to our observation of DrDV-B in *C. perspicillata*. For example, PmacDV from the Lesser dog-like bat clustered within the genetic diversity of PsemDV from rats, but infected two out of three individual bats analyzed, suggesting a recent cross-species transmission event followed by some currently unknown amount of onward transmission. Irrespective of the long-term outcomes of index infections, our results unequivocally support the conclusion that deltaviruses can transmit between divergent mammalian orders. The global distribution of deltavirus positive and negative datasets provides additional, independent evidence for host shifts. Even allowing for sub-

detection due to variation in infection prevalence and dataset quality, deltaviruses should have been more widespread across the mammalian phylogeny than we observed (ca. 1% of species analyzed) if they co-speciated with their hosts. Moreover, the three deltavirus-infected mammalian orders occur in both the New and Old Worlds, yet non-human deltaviruses occurred exclusively in the Americas. Sampling biases cannot readily explain this pattern. By most metrics of sequencing effort, Old World mammals were over-represented each deltavirus-infected mammalian order, including at finer continental scales (Supplementary Results, Section 1). Despite the large scale of our search, we evaluated < 10% of mammalian species. We therefore anticipate further discoveries of mammalian deltaviruses. Crucially, however, new viruses could not re-unite the paraphyletic rodent and bat deltaviruses or resolve widespread incongruence between mammal and deltavirus phylogenies, making our conclusions on host shifting robust.

The origin of HDV has been a longstanding mystery thwarted by the absence of closely related deltaviruses. The addition of 6 new mammalian deltaviruses by ourselves and others allowed us to re-evaluate this question (*7*, *10*). The pervasiveness of host shifting among deltaviruses and our discovery of a clade of mammalian deltaviruses basal to HDV (albeit with variable support depending on phylogeny, PP = 0.64-0.81) strongly points to a zoonotic origin. Although the exact progenitor virus remains undiscovered, the exclusive detection of mammalian deltaviruses in the New World species supports an "out of the Americas" explanation for origin and global spread of HDV (Fig. 1). The basal placement of the highly divergent Amazonian HDV genotype (HDV-3) within the phylogeny lends further credence to this scenario. Though circumstantial, the earliest records of HDV are from the Amazon basin in the 1930s (*19*). The greater diversity of HDV genotypes outside of the Americas – long argued to support an Old World origin – may instead reflect diversification arising from geographic vicariance within human populations.

Our results show that deltaviruses jump between mammalian host species through an unusual process that most likely requires parasitizing evolutionarily independent viruses. Since satellite viruses in general and HDV in particular tend to alter the pathogenesis and transmissibility of their helpers (*20*), our findings imply the potential for deltaviruses to act as host-switching virulence factors that could alter the progression of viral infections in multiple host species. Constraints on future host shifts are likely to differ from those of conventional

292 animal pathogens. Specifically, given the broad cellular tropism of deltaviruses, interactions with
293 helpers would likely be more important determinants of cross-species transmission than
294 interactions with their hosts (*17*, *18*). Consequently, anticipating future host shifts requires
295 understanding the determinants and plasticity of deltavirus and helper compatibility along with
296 the ecological factors that enable cross-species exposure.
297

298 **Acknowledgments**

299 We thank Jaime Pacheco, Luigi Carrasco, Yosselym Luzon, Saori Grillo and Megan Griffiths for
300 field and laboratory assistance; Megan Griffiths, Joseph Hughes, and Matt Hutchinson for
301 analysis advice; and Ana da Silva Filipe, Felix Drexler and Pablo Murcia for comments on
302 earlier versions of the manuscript. We thank the Serratus team, particularly Artem Babaian and
303 Robert Edgar for assistance with Serratus. **Funding:** Funding was provided by the Wellcome
304 Trust (Institutional Strategic Support Fund Early Career Researcher Catalyst Grant; Wellcome-
305 Beit Prize:102507/Z/13/A; Senior Research Fellowship: 102507/Z/13/Z), the Human Frontiers
306 Science Program (RGP0013/2018), and the Medical Research Council (MC_UU_12014/12).
307 Additional support was provided by the National Science Foundation (Graduate Research
308 Fellowship and DEB-1601052), ARCS Foundation, Sigma Xi, Animal Behavior Society, Bat
309 Conservation International, American Society of Mammalogists, Odum School of Ecology,
310 UGA Graduate School, UGA Latin American and Caribbean Studies Institute, UGA Biomedical
311 and Health Sciences Institute, and the Explorer's Club. **Competing interests:** Authors declare no
312 competing interests. **Data and materials availability:** DrDV genome sequences are available on
313 Genbank (accessions MT649206- MT649209). PmacDV, OvirDV and MmonDV genome
314 sequences are available at https://serratus.io/access. Peruvian bat metagenomes are available in
315 ENA project PRJEB35111. Scripts used for bioinformatic analyses are available on GitHub
316 (https://github.com/rjorton/Allmond). **Author contributions:** Conceptualization (LMB, RJO,
317 AHP, RB, DGS); formal analysis (LMB, RJO, DGS), funding acquisition (LMB, DGS);
318 investigation (LMB, AB); resources (DJB, CT, JEC); supervision (AHP, RB, DGS); writing –
319 original draft (LMB, DGS); all authors contributed to review and editing of the manuscript.

320 **Supplementary Materials:**

321 Materials and Methods

322 Supplementary Results

323 Figures S1-S8

324 Tables S1-S6

325 Supplementary References
326

327

328

References

1. L. Magnius *et al.*, ICTV Virus Taxonomy Profile: Deltavirus. *J Gen Virol.* **99**, 1565–1566 (2018).

2. K. Salehi-Ashtiani, A. Lupták, A. Litovchick, J. W. Szostak, A genomewide search for ribozymes reveals an HDV-like sequence in the human CPEB3 gene. *Science*. **313**, 1788–1792 (2006).

3. S. F. Elena, J. Dopazo, R. Flores, T. O. Diener, A. Moya, Phylogeny of viroids, viroidlike satellite RNAs, and the viroidlike domain of hepatitis delta virus RNA. *Proc Natl Acad Sci USA.* **88**, 5631–5634 (1991).

4. M. Wille *et al.*, A Divergent Hepatitis D-Like Agent in Birds. *Viruses*. **10**, 720–9 (2018).

5. U. Hetzel *et al.*, Identification of a Novel Deltavirus in Boa Constrictors. *mBio*. **10**, 1447–8 (2019).

6. W.-S. Chang *et al.*, Novel hepatitis D-like agents in vertebrates and invertebrates. *Virus Evol*. **5**, vez021 (2019).

7. S. Paraskevopoulou *et al.*, Mammalian deltavirus without hepadnavirus coinfection in the neotropical rodent Proechimys semispinosus. *Proc Natl Acad Sci USA.* **117**, 17977–17983 (2020).

8. M. Shi *et al.*, Redefining the invertebrate RNA virosphere. *Nature*. **540**, 539–543 (2016).

9. M. Shi *et al.*, The evolutionary history of vertebrate RNA viruses. *Nature*. **556**, 197–202 (2018).

10. R. C. Edgar *et al.*, Petabase-scale sequence alignment catalyses viral discovery. *bioRxiv*, 1–30 (2020).

11. L. M. Bergner *et al.*, Using noninvasive metagenomics to characterize viral communities from wildlife. *Mol Ecol Resour*. **19**, 128–143 (2019).

12. D. D. Moreno-Santillán, C. Machain-Williams, G. Hernández-Montes, J. Ortega, De Novo Transcriptome Assembly and Functional Annotation in Five Species of Bats. *Sci Rep.* **9**, 6222–12 (2019).

13. C. M. Seabury *et al.*, Genome-Wide Polymorphism and Comparative Analyses in the White-Tailed Deer (Odocoileus virginianus): A Model for Conservation Genomics. *PLOS ONE*. **6**, e15811–9 (2011).

14. S. P. Fletcher *et al.*, Intrahepatic Transcriptional Signature Associated with Response to Interferon-α Treatment in the Woodchuck Model of Chronic Hepatitis B. *PLoS Pathog*. **11**, e1005103–30 (2015).

15. J. Krushkal, W. H. Li, Substitution rates in hepatitis delta virus. *J Mol Evol*. **41**, 721–726 (1995).

16. J. F. Drexler *et al.*, Bats carry pathogenic hepadnaviruses antigenically related to hepatitis B virus and capable of infecting human hepatocytes. *Proc Natl Acad Sci USA.* **110**, 16151–16156 (2013).

17. J. Perez-Vargas *et al.*, Enveloped viruses distinct from HBV induce dissemination of hepatitis D virus in vivo. *Nat Commun*. **10**, 2098 (2019).

18. L. Szirovicza *et al.*, Snake Deltavirus Utilizes Envelope Proteins of Different Viruses To Generate Infectious Particles. *mBio*. **11** (2020), doi:10.1128/mBio.03250-19.

19. M. V. Alvarado-Mora *et al.*, Dynamics of hepatitis D (delta) virus genotype 3 in the Amazon region of South America. *Infect Genet Evol.* **11**, 1462–1468 (2011).

20. P. Gnanasekaran, S. Chakraborty, Biology of viral satellites and their role in pathogenesis. *Curr Opin Virol*. **33**, 96–105 (2018).

Supplementary Materials for

Diversification of mammalian deltaviruses by host shifting

Laura M. Bergner, Richard J. Orton, Alice Broos, Carlos Tello, Daniel J. Becker, Jorge E. Carrera, Arvind H. Patel, Roman Biek, Daniel G. Streicker

This file includes:

Materials and Methods

1. Virus discovery

a. Serratus

The Serratus platform was used to search published mammalian metagenomic and transcriptomic sequence datasets available in the NCBI Short Read Archive (SRA). Briefly, Serratus uses a cloud computing infrastructure to perform ultra-high throughput alignment of publicly available SRA short read datasets to viral genomes of interest (*1*). Due to the exceptional computational demands of this search and mutual interest between ourselves and another research team, Serratus searches were designed by both teams and carried out at the protein and nucleotide levels by Edgar *et al.* (*1*). Query sequences for Serratus searches included all HDV genotypes and all deltavirus-like genomes which were publicly available at the time of the search (July 2020) along with representative genomes from DrDV-A and DrDV-B, which our team had already discovered. Results were shared among the two teams who subsequently pursued complementary lines of investigation. Novel mammalian deltaviruses were discovered using nucleotide (OvirDV) and amino acid level (Mmon DV and PmacDV) searches of the mammalian SRA search space.

b. Neotropical bat metagenomic sequencing

Total nucleic acid was extracted from archived saliva swabs from Neotropical bats on a Kingfisher Flex 96 automated extraction machine (ThermoFisher Scientific) with the Biosprint One-for-all Vet Kit (Qiagen) using a modified version of the manufacturer's protocol as described previously (*2*). Ten pools of nucleic acids from vampire bats and other bat species were created for shotgun metagenomic sequencing (Table S1). Eight pools comprised samples from bats in the same genus (2-10 individuals per pool depending on availability of samples, 30 µL total nucleic acid per individual). The CAJ1 vampire bat pool from (*3*) which contained deltavirus reads was included as a sequencing control. The final pool ("Rare species") comprised 8 other bat species that had only one individual sampled each. Pools were treated with DNAse I (Ambion) and purified using RNAClean XP beads (Agencourt) following (*2*). Libraries were prepared using the SMARTer Stranded Total RNA-Seq Kit v2 - Pico Input Mammalian (Clontech) and sequenced on an Illumina NextSeq500 at The University of Glasgow Polyomics Facility. Samples were bioinformatically processed for viral discovery as described previously

(*2*), with a slight modification to the read trimming step to account for shorter reads and a different library preparation kit.

c. DrDV genome assembly and annotation

DrDV genomes were assembled using SPAdes (*4*) and refined by mapping cleaned reads back to SPAdes-generated contigs within Geneious v 7.1.7 (*5*). Regions of overlapping sequence at the ends of genomes due to linear *de novo* assemblies of circular genomes were resolved manually. Genome circularity was confirmed based on the presence of overlapping reads across the entire circular genome of both DrDVs. The amino acid sequence of the small delta antigen protein (DAg) was extracted from sequences using getorf (*6*). Other smaller identified open reading frames did not exhibit significant homology when evaluated by protein blast against Genbank. Nucleotide sequences of full deltavirus genomes and amino acid sequences of DAg were aligned along with representative sequences from other deltaviruses using the E-INS-i algorithm in MAFFT v 7.017 (*7*). Genetic distances as percent identities were calculated based on an untrimmed full genome alignment of 2,321bp and an untrimmed delta antigen alignment of 281aa. Protein domain homology of the DAg was analyzed using Hhpred (*8*). Ribozymes were identified manually by examining the region upstream of the delta antigen open reading frame where ribozymes are located in other deltavirus genomes (*9, 10*). RNA secondary structure and self-complementarity were determined using the webservers for mFold (*11*) and RNAStructure (*12*). We found no evidence of recombination in nucleotide alignments of DrDV DAg according to the program GARD (*13*) on the Datamonkey webserver (*14*). Genome assembly and annotation of PmacDV, OvirDV, and MmonDV are described in (*1*).

d. Evaluation of deltavirus positive cohorts

To establish that deltaviruses were likely to be actively infecting hosts in which they were detected, and not laboratory contamination or incidental detection of environmentally derived RNA, we searched for evidence of deltavirus infections in additional samples from the various studies that detected full genomes. Samples included sequencing libraries derived from both different individuals in the same study and different tissues from the same individuals. Searches used bwa (*15*) to map raw reads from deltavirus positive cohorts to the corresponding novel deltavirus genomes which had been detected in those same cohorts. Genome remapping was performed for all vampire bat libraries, two other *Peropteryx macrotis* libraries and all other Neotropical bat species sequenced in the same study (*16*) and other pooled tissue samples

sequenced by RNASeq from *Odocoileus virginianus* in the same study (*17*). Results are shown in Table S2. Deltavirus reads from additional individuals and timepoints from the *Marmota monax* study (*18*) are described in (*1*).

e. Global biogeographic analysis of deltavirus presence and absence

To characterize the global distribution of mammal-infecting deltaviruses, we used the metadata of each SRA accession queried in the Serratus search to identify the associated host. We focused primarily on the mammalian dataset, which was generated by the SRA search query ("Mammalia"[Organism] NOT "Homo sapiens"[Organism] NOT "Mus musculus"[Organism]) AND ("type_rnaseq"[Filter] OR "metagenomic"[Filter] OR "metatranscriptomic"[Filter]) AND "platform illumina"[Properties]. All analyses were performed in R version 3.5.1 ((*19*). We removed libraries with persistent errors which had not completed in the Serratus search. For remaining libraries, when host identification information was available to the species level, we matched Latin binomial species names to Pantheria, a dataset which contains the centroids of mammalian geographic distributions, and used an R script to assign species to continents using these geographic data (*20*). Subspecies present in scientific names of SRA meta-data were re-assigned to species level and recently updated binomial names were changed to match the Pantheria dataset. Due to the fact that mammalian taxonomic data in Pantheria date to 2005, some former Orders which are no longer in use (e.g. Soricomorpha) appear in our data but are not expected to affect the results of analyses. Forty-eight species whose centroids occurred in water bodies were assigned to continents by manually inspecting species ranges. Widely-distributed domesticated animals, datasets with genus-level metadata from broadly-distributed genera, datasets from cell lines or with taxonomic information only at the Class level, and those which had no geographic range data available (mostly aquatic mammals) were searched by Serratus, but excluded from geographic comparisons. We quantified geographic and taxonomic biases in our dataset both in units of bases of RNA sequenced and number of species investigated.

Although most mammalian metagenomic and transcriptomic libraries were captured in the mammalian search, we also examined datasets from SRA search queries for vertebrates, metagenomes, and viromes to ensure that all relevant libraries were captured in our measures of search effort. For these datasets, we removed libraries with persistent errors and calculated search effort as bases of RNA sequenced across the three orders in which deltaviruses were

discovered, removing libraries named for specific viral taxa which may have been enriched for these taxa and therefore do not represent a likely source of novel viruses. As these libraries lacked species-level meta-data (hence their exclusion from the mammalian search above), we could not systematically calculate number of species in these datasets. Additional search queries are available at https://github.com/ababaian/serratus/wiki/SRA-queries.

2. Phylogenetic analyses

a. Bayesian phylogeny using MrBayes

Phylogenetic analysis was performed on complete DAg amino acid sequences to place mammalian deltaviruses relative to HDV and other described deltaviruses. Representative sequences from each clade of HDV and other previously published DVs were aligned with DrDVs (sequences generated by RT-PCR, described in Methods section 3b), PmacDV, OvirDV and MmonDV using the E-INS-i algorithm and JTT2000 scoring matrix of MAFFT within Geneious. Large delta antigen sequences from HDV were trimmed manually to small delta antigen length, and the alignment was further trimmed in trimal using the automated1 setting to a final length of 192aa. The best substitution model (JTTDCMut+F+G4) was determined using ModelFinder (*21*) within IQTree 2 (*22*). Bayesian phylogenetic analysis was performed using the most similar model available within MrBayes (JTT+F+G4). The analysis was run for 5,000,000 generations and sampled every 2,500 generations, with the first 500 trees discarded as burn-in to generate the consensus tree.

b. Bayesian phylogeny using StarBeast

We used StarBeast to generate a species-level phylogeny for the co-phylogenetic analysis, using the same amino acid alignment of complete DAg which was used in the MrBayes analysis. StarBeast is typically used with multi-locus sequence data from multiple individuals per species but can also be applied to single gene alignments (*23*). Notably, a preliminary analysis suggested this approach was more conservative than a constant effective size coalescent model in BEAST which substantially inflated posterior probabilities on nodes across the tree relative to the MrBayes analysis (Fig. 2A). The StarBeast multi-species coalescent analysis was carried out as two duplicate runs of 50 million generations (sampling every 5000 generations) in BEAST2, using the JTT+G substitution model, the linear with constant root model for the species tree population size, and a Yule speciation model. Combined log files were assessed for convergence

and effective sample size values >200 using TRACER. Twenty percent of trees were discarded as burn-in prior to generating the consensus tree.

c. Co-phylogeny

Co-phylogenetic analyses were performed in R using PACo (*24*, *25*) and ParaFit (*26*, *27*). Analyses were performed on three subsets of matched host-deltavirus data: all taxa, ingroup taxa (mammals, bird and snake) and mammals only. Host datasets consisted of distance matrices derived from a TimeTree phylogeny (timetree.org). For metagenomic libraries which contained individuals of multiple species (AvianDV and FishDV), one host was selected for inclusion (*Anas gracilis* and *Macroramphosus scolopax*, respectively). Host data were not available in TimeTree for two species in which deltaviruses were discovered (*Proechimys semispinosus* and *Schedorhinotermes intermedius*), so available congeners were substituted (*Proechimys guairae* and *Schedorhinotermes medioobscurus*, respectively). Virus datasets consisted of distances matrices from posterior species trees generated in StarBeast. Co-phylogeny analyses performed using virus distance matrices derived from posterior MrBayes trees, pruned to contain only relevant taxa, yielded qualitatively similar results. For both analyses, the principal coordinates analysis of distance matrices was performed with the 'cailliez' correction. Since units of branch length differed between host and virus trees, all distance matrices were normalized prior to co-evolutionary analyses. To account for phylogenetic uncertainty in the evolutionary history of deltaviruses, analyses were carried out using 1,000 trees randomly selected from the posterior distribution of the Bayesian phylogenetic analyses (separately for StarBeast and MrBayes). Due to uncertain placement of HDV3 in both phylogenies, one representative of HDV was randomly selected for each iteration. For each tree, we calculated summary statistics (see below) describing the dependence of the deltavirus phylogeny on the host phylogeny. *P*-values were estimated using 1,000 permutations of host-virus associations.

For PACo analyses, the null model selected was r0, which assumes that virus phylogeny tracks the host phylogeny. Levels of co-phylogenetic signal were evaluated as the median global sum of squared residuals ($m2_{xy}$) and mean significance (*P*-values), averaged over the 1,000 posterior trees. Empirical distributions were compared to null distributions for each dataset. For ParaFit analyses, the levels of co-phylogenetic signal in each dataset were evaluated as the median sum of squares of the fourth corner matrix (ParaFitGlobal) and mean significance (*P*-values), averaged over 1,000 posterior trees. ParaFit calculates the significance of the global

host-virus association statistic by randomly permuting hosts in the host-virus association matrix to create a null distribution. Since Parafit does not provide this distribution to users, we approximated it for visualization by manually re-estimating the global host-virus association statistic for 1,000 random permutations of hosts in the host-virus association matrix. Phylogenies and co-phylogenies were visualized in R using the packages 'ape' (*27*), 'phangorn' (*28*), 'phytools' (*29*), and 'ggtree' (*30*).

3. Deltaviruses in Neotropical bats

a. Capture and sampling of wild bats

To examine DrDV prevalence in vampire bats, we studied 12 sites in three departments of Peru between 2016-2017 (Fig. 3A). Age and sex of bats were determined as described previously (*2*). Saliva samples were collected by allowing bats to chew on sterile cotton-tipped wooden swabs (Fisherbrand). Blood was collected from vampire bats only by lancing the propatagial vein and saturating a sterile cotton-tipped wooden swab with blood. Swabs were stored in 1 mL RNALater (Ambion) overnight at 4°C before being transferred to dry ice and stored in -70°C freezers.

Bat sampling protocols were approved by the Research Ethics Committee of the University of Glasgow School of Medical, Veterinary and Life Sciences (Ref081/15), the University of Georgia Animal Care and Use Committee (A2014 04-016-Y3-A5), and the Peruvian Government (RD-009-2015-SERFOR-DGGSPFFS, RD-264-2015-SERFOR-DGGSPFFS, RD-142-2015-SERFOR-DGGSPFFS, RD-054-2016-SERFOR-DGGSPFFS).

b. RT-PCR and sequencing of blood and saliva samples

Primers were designed to screen bat saliva and blood samples for a conserved region of the DAg protein of DrDV-A (236bp) and DrDV-B (231bp), by hemi-nested and nested RT-PCR respectively (Table S4). Alternative primers were designed to amplify the complete DAg for DrDV-A (707bp) and DrDV-B (948bp) using a one-step RT-PCR (Table S4). cDNA was generated from total nucleic acid extracts using the Protoscript II First Strand cDNA synthesis kit with random hexamers; RNA and random hexamers were heated for 5 minutes at 65°C then placed on ice. Protoscript II reaction mix and Protoscript II enzyme mix were added to a final concentration of 1x, and the reaction was incubated at 25°C for 5 minutes, 42°C for 15 minutes, and 80°C for 5 minutes. PCR was performed using Q5 High-Fidelity DNA Polymerase (NEB). Each reaction contained 1x Q5 reaction buffer, 200 μM dNTPs, 0.5 μM each primer, 0.02 U/μL

Q5 High Fidelity DNA polymerase and either 2.5 µL cDNA or 1 µL Round 1 PCR product. Reactions were incubated at 98°C for 30 seconds, followed by 40 cycles of 98°C for 10 seconds, 61-65°C for 30 seconds (or 58-60°C for 30 seconds for the complete DAg), 72°C for 40 seconds, and a final elongation step of 72°C for 2 minutes. PCR products of the correct size were confirmed by re-amplification from cDNA or total nucleic acid extracts and/or Sanger sequencing (Eurofins Genomics).

c. Bat species confirmation

We confirmed the morphological species assignment of the *C. perspicillata* individual in which DrDV-B was detected by sequencing cytochrome B. Cytochrome B was amplified from the same saliva sample in which DrDV-B was detected using primers Bat 05A and Bat 04A (*31*) and GoTaq Green Master Mix (Promega) according to the manufacturer's instructions, and the resulting product was Sanger sequenced (Eurofins Genomics) then evaluated by nucleotide blast against Genbank.

d. Genetic diversity and distribution of DrDV-B

To examine relationships among DrDV-B sequences, Bayesian phylogenetic analysis was performed on a 214bp fragment of the DAg. Sequences from saliva and blood of 41 *D. rotundus* and saliva from one *C. perspicillata* were aligned using MAFFT within Geneious. Duplicate sequences originating from the blood and saliva of the same individuals were removed. Alignments were trimmed using Trimal (*32*) with automated1 settings, and the best model of sequence evolution was determined using jModelTest2 (*33*). Phylogenetic analysis was performed using MrBayes 3.6.2 (*34*) with the GTR+I model. The analysis was run for 4,000,000 generations and sampled every 2,000 generations, with the first 1,000 trees removed as burn-in. The association between phylogenetic relationships and location at both the regional and colony level was tested using BaTS (*35*) with 1,000 posterior trees and 1,000 replicates to generate the null distribution.

e. Statistical analyses of DrDV-B

We modeled the effects of age and sex on DrDV-B presence in saliva using a binomial generalized linear mixed model (GLMM) in the package lme4 (*36*) in R. Age (female/male) and sex (adult/subadult) were modeled as categorical variables, with site included as a random effect. We also evaluated differences in DrDV-B prevalence between regions of Peru using a binomial

generalized linear model (GLM), and used the *Anova* function of the *car* package (*37*) to calculate the likelihood ratio χ_2 test statistic.

4. Identifying candidate helper viruses for mammalian deltaviruses

a. Hepadnavirus screening in vampire bats

We tested samples for the presence of bat hepadnavirus as a candidate helper virus to DrDV. DNA from saliva and blood samples was screened for HBV-like viruses using pan-*Hepadnaviridae* primers (HBV-F248, HBV-R397, HBV-R450a, HBV-R450b; Table S4) and PCR protocols (*38*). We used a plasmid carrying a 1.3-mer genome of human HBV that is particle assembly defective but replication competent as a positive control.

b. Bioinformatic screening of published metagenomic datasets

We performed comprehensive virus discovery using an in-house bioinformatic pipeline (*2*) on sequence datasets containing deltaviruses to identify candidate helper viruses. Datasets analyzed included all vampire bat datasets (22 from (*2*), 46 from (*3*)), *P. macrotis* datasets (SRR7910142, SRR7910143, SRR7910144), *O. virginianus* datasets (SRR4256025-SRR4256034), and *M. monax* datasets (SRR2136906, SRR2136907). Briefly, after quality trimming and filtering, reads were analyzed by blastx using DIAMOND (*39*) against a RefSeq database to remove bacterial and eukaryotic reads. Remaining reads were then *de novo* assembled using SPAdes (*4*) and resulting contigs were analyzed by blastx using DIAMOND against a non-redundant (NR) protein database (*40*). KronaTools (*41*) and MEGAN (*42*) were used to visualize and report taxonomic assignments.

Supplementary Results

1. Evaluation of continent level geographic biases in Serratus data

We sought to confirm that the sole detection of mammalian deltaviruses in the Americas in three different mammalian orders was unlikely to have arisen from sampling biases in the RNA sequence datasets that we analyzed. The main text illustrates geographic patterns at broad scales and shows that New World species were under-represented relative to Old World species, indicating that sampling biases were unlikely to explain the absence of deltaviruses from Old World species. However, we also examined biases at finer geographic and taxonomic scales, focusing on the mammalian SRA search query dataset for which there was species and continent level information. At the continent level, data volumes (in bases of RNA sequenced) declined

638 from Asia (6.35e13), Africa (2.89e13), South America (7.99e12), North America (4.93e12),
639 Europe (4.86e12), to Australia (3.75e12) (Fig S7). This implies that Africa (the previously
640 assumed origin of HDV) has more than double the data of the Americas combined. Similar
641 patterns were evident within the deltavirus-infected mammalian orders. For Artiodactyla, North
642 and South American datasets were ranked 3rd and 5th respectively among the 5 continents which
643 had sequence data. Although there was less Artiodactyla data from Africa than North America,
644 Asia (1st) and Europe (2nd) had 2 and 1.6-fold more data than the Americas combined. For bats,
645 North and South American datasets were ranked 5th and 6th among the 6 continents with data,
646 and Europe (1st) and Africa (2nd) had 2.5 and 1.2-fold more data than datasets combined across
647 the Americas. For rodents, North America datasets were ranked 2nd, while South American
648 datasets were ranked 5th out of the 5 continents with data, but Asia (1st) had 1.1-fold more data
649 than the Americas combined and Africa had 3.6 times more data than South America.
650 We also examined potential biases in search effort by number of species sequenced per
651 continent. There were equal or fewer species of Artiodactyla sequenced in North (N = 5) and
652 South America (N=1) compared to Europe (N = 5), Asia (N = 8) and Africa (N = 14). Similarly,
653 rodent species sampled from Old World continents (N = 48; Europe [N = 8], Africa [N = 14],
654 and Asia [N = 26]) outnumbered those in the New World (N = 33; North America [N = 21],
655 South America [N = 12]. Neither Rodentia nor Artiodactyla datasets were searched from
656 Australia. In contrast, there were more bat species in North and South American datasets (N = 4
657 and 42, respectively) compared to Asia (N = 22), Africa (N = 5), Europe (N = 2), and Australia
658 (N =1) leading to a slight bias toward New World bats (46 species vs 30 Old World species).
659 Consequently, in the 'mammalian' dataset, New World bats were more numerous at the species
660 level, but had fewer individuals tested per species and/or less sequencing depth per species.
661 We further examined datasets generated by related search queries (vertebrate, metagenome
662 and virome) which included some libraries from mammals that were excluded from the
663 'mammalian' dataset (see Materials and Methods, Section 1e). The vertebrate dataset contained
664 no matches to the three mammalian Orders of interest (Rodentia, Artiodactyla, Chiroptera). For
665 Rodentia, the metagenome dataset contained 380 libraries (9.7e7 bases) identified as "mouse
666 metagenome" and the virome dataset contained 171 libraries (1e11 bases) which were identified
667 as "mouse gut metagenome" or "rodent metagenome" or "Rattus" or "rat gut metagenome".
668 These could not be assigned geographic provenance and likely represented laboratory animals.

For Artiodactyla, the virome dataset contained 317 libraries (1e11 bases) which were identified as "pig gut metagenome" or "pig metagenome" or "bovine gut metagenome". As these libraries likely derived from either experimental or domestic animals, we conclude that additional data from these two Orders are unlikely to influence geographic or taxonomic bias. For Chiroptera, there were a total of 25 libraries (2.4e10 bases) identified as "bat metagenome". The vast majority (N=24) were from Old World bats. Eleven derived from a study of bat rotaviruses (PRJNA562472) which of which 10 were collected from Old world locations (Ghana, Bulgaria) and one from New World (Costa Rica). Two libraries were bat viral metagenomes generated from samples collected in South Africa (SRR5889194; SRR5889129), and twelve libraries were generated from bats sampled in China (PRJNA379515). There were 14 bat species analyzed in all of these libraries, of which eight were not included in the mammalian SRA dataset, bringing the total number of Old World bat species to 38. Therefore, by the metric of number of species, New World bats remained slightly over-represented (38 versus 46 species) though as mentioned above, Old World bat derived datasets were sequenced more comprehensively and covered a larger number of continents.

Overall, across the three orders in which we detected deltaviruses, fewer species were studied in North and South American datasets (85 species) compared to those from Africa, Asia, Europe and Australia (105 species) and the total volume of RNA sequenced was 2.7 times greater for Old world species (1.64e13 bases RNA) than New world species (6.02e12). We therefore conclude that the exclusive presence of deltaviruses in American mammals is unlikely to represent geographic biases in our datasets.

2. Large delta antigen in novel mammalian deltaviruses

In HDV, the large delta antigen protein (L-HDAg) is produced by RNA editing of the UAG stop codon to include 19 additional aa (*43*) and contains a farnesylation site which interacts with HBV (*44*). The DrDV-B DAg from the genome from bat colony CAJ1 terminated in UAG, which if edited similarly to HDV would generate a putative L-DAg containing an additional 28 aa (Fig. S3). In contrast, DrDV-B DAg from the two other bat colonies from which genomes were sequenced (LMA6 and AYA11), as well as DrDV-A DAg, terminated in a UAA stop codon so would not appear to be similarly edited, although it is possible to extend the open reading frames through frameshifting (*9*). Importantly, no putative vampire bat L-DAg generated

699 through either RNA editing or frameshifting contained a farnesylation site. PmacDV, OvirDV,
700 and MmonDV also did not contain apparent L-DAg extensions or farnesylation sites (*1*).

701 **3. Co-phylogenetic results across posterior distributions of trees from two Bayesian**
702 **searches and two different co-phylogeny analyses**

703 Consensus topologies differed slightly between the phylogenetic analyses of deltaviruses using a
704 multi-species coalescent model in StarBeast and a coalescent model in MrBayes, particularly in
705 relation to the termite-associated deltavirus-like agent and avian deltavirus (compare Fig. 2A and
706 2B). We therefore repeated our co-phylogenetic analysis using 1,000 trees from the MrBayes
707 analysis to verify that our conclusions were robust to this topological inconsistency. Analyses
708 performed using virus distance matrices derived from posterior MrBayes trees were congruent
709 with those in StarBeast.

710 In the broadest analyses of all taxa, results differed slightly among co-phylogenetic
711 analyses. Specifically, PACo analyses supported the dependence of the deltavirus phylogeny on
712 the host phylogeny (StarBeast trees: m^2_{xy} = 0.57 (standard deviation = 0.48- 0.66); $m^2_{xy\_null}$ =
713 1.27 (1.11- 1.44); *P* = 0.01; MrBayes trees: (m^2_{xy} = 0.53 (0.46- 0.6); $m^2_{xy\_null}$ = 1.26 (1.1- 1.42); *P*
714 = 0.002). However, ParaFit analyses supported independence of the virus and host phylogenies
715 based on both StarBeast trees (ParaFitGlobal = 0.72 (standard deviation = 0.59- 0.86); *P*= 0.09)
716 and MrBayes trees (ParaFitGlobal = 0.63 (0.52- 0.75); *P*= 0.07). Similarly, for ingroup taxa
717 (mammalian, avian and snake deltaviruses), PACo detected evidence of co-phylogeny using both
718 sets of trees (Starbeast: m^2_{xy} = 0.81 (0.66- 0.96); $m^2_{xy\_null}$ = 1.3 (1.14- 1.46); *P* = 0.02; MrBayes:
719 m^2_{xy} = 0.76 (0.69- 0.83); $m^2_{xy\_null}$ = 1.28 (1.1- 1.46); *P* = 0.01), while ParaFit analyses with
720 StarBeast trees (ParaFitGlobal = 0.8 (0.7- 0.89); *P*= 0.12) and MrBayes trees (ParaFitGlobal =
721 0.68 (0.62- 0.75); *P*= 0.09) found no significant support for co-phylogeny.

722 All analyses of mammalian deltaviruses failed to reject the null hypothesis of independence
723 of phylogenies. These results were consistent when with both StarBeast and MrBayes trees in
724 PACo (StarBeast: m^2_{xy} = 1.51 (1.36- 1.65); $m^2_{xy\_null}$ = 1.66 (1.43- 1.9); *P* = 0.28; MrBayes: m^2_{xy}
725 = 1.16 (1.07- 1.25); $m^2_{xy\_null}$ = 1.22 (0.97- 1.48); *P* = 0.35), as well as in ParaFit (StarBeast:
726 ParaFitGlobal = 0.61 (0.55- 0.68); *P*= 0.52; MrBayes: ParaFitGlobal = 0.49 (0.44- 0.54); *P*=
727 0.5).

728 In summary, both PACo and ParaFit analyses of StarBeast and MrBayes trees showed no
729 support for co-phylogeny in the mammalian dataset. Including more divergent host-virus pairs

increased support for co-phylogeny in the all taxa and ingroup datasets, with these results being statistically significant in PACo analyses but not in ParaFit analyses. Inconsistent support for phylogenetic independence at broader scales may reflect variation in the sensitivity of different analyses to detect phylogenetic congruence which occurs in only a subset of branches. For example, the non-ingroup deltavirus-like agents formed a polytomy of long branches and were found in the most divergent hosts from mammals, which may have inflated co-phylogenetic signal (Fig. S5). Regardless, given the consistent evidence against a co-speciation model among mammals and incongruences observed among other taxa in the consensus topologies, these findings illustrate that a model of co-speciation alone cannot explain the evolutionary relationships of deltaviruses and their hosts.

4. Putative cross-species transmission of DrDV-B to a frugivorous bat.

The detection of a vampire bat associated deltavirus in a frugivorous bat (*Carollia perspicillata)* is strongly suggestive of cross-species transmission but might also arise through mis-assignment of bat species in the field or contamination of samples during laboratory processing. To exclude the possibility of host species mis-identification, we confirmed morphological species assignment by sequencing Cytochrome B from the same saliva sample in which we amplified deltavirus (see Methods), which showed 99.49% identity with a published *C. perspicillata* sequence in Genbank (Accession AF511977.1). Laboratory contamination was minimized by processing all samples through a dedicated PCR pipeline with a one directional workflow. PCR reagents are stored and master mixes prepared in a laboratory that is DNA/RNA free, and which cannot be entered after going into any other lab. Field collected samples from bats are extracted and handled in a room strictly used for clinical samples which cannot be entered after going in any other lab aside from the master mix room. To further exclude laboratory contamination, we independently amplified the *C. perspicillata* deltavirus product from two separate batches of cDNA. We used only round 1 primers of a nested PCR to avoid detecting trace amounts of potential contamination; in vampire bats only 68% of individuals deemed positive after round 2 were also positive in round 1. Furthermore, in the laboratory, samples from other bat species were handled separately from samples collected from vampire bats, with extractions and PCRs being performed on different days. As discussed in the main text, the absence of genetic divergence from sympatric strains in *D. rotundus* indicates limited or no onward transmission of DrDV-B in *C. perspicillata*. Whether the *C. perspicillata* sustained an actively replicating

761 infection is uncertain, although detection in a single round of PCR (which was true for only 68%
762 of DrDV-positive vampire bats) implies an intensity of infection which could suggest DrDV
763 replication in the recipient host, though this would require further testing to confirm. Definitively
764 resolving the extent of DrDV-B replication could be achieved using a quantitative RT-PCR
765 targeting the DrDV antigenome. Such assays do not currently exist and after the confirmatory
766 testing above, in addition to metagenomic sequencing, we unfortunately would no longer have
767 sufficient RNA available from the *C. perspicillata* bat to run such a test if it were available. In
768 summary, we are confident that the individual in which the deltavirus was detected is a *C.*
769 *perspicillata* and we believe the most likely explanation to be cross-species transmission in
770 nature, though whether this represents an active infection remains uncertain.

771 **5. Candidate helper viruses of OvirDV and MmonDV**

772 We also examined viral communities in *O. virginianus* and *M. monax* libraries for candidate
773 helpers. Given that MmonDV was detected in animals experimentally inoculated with
774 Woodchuck Hepatitis Virus (WHV, a Hepadnavirus), these libraries were unsurprisingly
775 dominated by WHV, but also contained reads matching to Herpesviridae, Flaviviridae,
776 Poxviridae and Retroviridae (Figure S8). *O. virginianus* libraries contained Poxviridae,
777 Retroviridae, and Herpesviridae reads. Consequently, reads matching to Poxviridae were
778 detected in libraries for all deltavirus hosts which were studied here (DrDV-A, DrDV-B,
779 PmacDV, MmonDV, OvirDV), although reads were less abundant than other viral taxa and
780 could not always be decisively ruled out as false positives. Although there is no experimental
781 evidence that Poxviruses can produce infectious deltavirus particles, this ecological association
782 may be worth considering in future studies of mammalian deltaviruses.

Supplementary Figures

	U81989	AB118846	AB118845	AM183326	AM183329	AM183333	AM183327	AB037948	OvirDV	MmonDV	DrDV-A	PmacDV	MK598009	DrDV-B	NC_040729	NC_040845	MN031240	MN031239	MK962760	MK962759
U81989_HDV1		73.5	72.3	69.6	68.3	68.9	71.2	60.4	57.8	51.5	53	46.8	46.8	47.5	41.8	37.2	31.9	30.7	28.1	30.1
AB118846_HDV2	73		76	74.7	74.1	71.5	72.5	62.5	58.7	52.6	54.5	47.5	47.4	48.2	42	37.5	33.2	31.7	28.5	30.2
AB118845_HDV4	74.4	75.7		74.3	72.6	71.5	72.9	63.1	61.5	53.4	56.1	48	48	49	41.8	37.4	32.9	30.4	27.8	29.9
AM183326_HDV5	70.9	77.1	75.3		74.7	72.6	72.1	61	58.6	51.2	55.1	47.8	47.8	48	42.4	37.8	32.2	31.5	28.3	30.7
AM183329_HDV6	69.3	72	69.6	76.3		71.9	72.3	62.4	59.2	52.8	54.5	47.9	47.8	48.1	41.8	35.7	32.1	31.4	27.7	31.2
AM183333_HDV7	68	72.6	70.2	77.3	72.6		75.4	60.9	58.7	51.1	52.1	46.9	46.9	47.3	42.8	36.3	31.2	31	27.9	30.1
AM183327_HDV8	68.9	72.4	75.7	79.9	75.8	75.4		61.5	58.9	52.2	53.6	47.6	46.9	47.5	42.1	35.7	31.1	31.1	26.3	30.4
AB037948_HDV3	66.8	63.2	66.1	65.7	64.6	63.3	64.7		55	50.6	52	46.5	46.1	46.7	41.4	35.7	30.1	29.8	26.7	30.1
OvirDV	61	64.1	69.1	65.1	66.1	62.7	65.6	63		55.8	61.6	47	47.4	47.1	42.7	35.8	31.2	31.1	25.7	28.2
MmonDV	55.4	57.4	60.3	56.4	54.7	54.5	54.9	59.4	67		56.9	45.8	46.2	45.9	43.5	33.7	28.5	29.4	23.4	27.4
DrDV-A	62.6	63.6	64.4	62.6	61.4	60.1	60.5	60.4	74.7	70.1		47	47.4	47.6	43.3	36.3	29	28.5	24.4	27.5
PmacDV	54.3	53.8	55.6	52.3	52.6	52.9	54.3	53.7	57.7	55.1	56.1		95.4	71.2	44.4	33.7	29	30	24.7	26.2
MK598009_PsemDV	54.8	53.8	56.1	52.8	54.2	53.4	54.8	54.7	58.2	55.1	56.1	96.9		72.6	43.8	33.7	29.4	30.1	24.2	26.3
DrDV-B_CAJ1	52.8	51.8	53.1	51.8	51.6	49.9	52.3	54.2	56.1	55.1	56.7	79.6	81.1		43.7	34.5	29.7	29.6	24.7	27.3
NC_040729_SnakeDV	50	47.2	47.7	46.2	47.8	45.9	45.2	47.8	50.8	50.3	51.8	53	54.5	53		34.2	28.7	27.1	23.2	26.2
NC_040845_AvianDV	40.7	36.2	39.4	36.7	35.7	37.9	36.2	38.9	37.2	39.9	38.3	34.7	35.3	37.9	34.9		25.7	30.4	24.9	25.4
MN031240_FishDV	19.8	18.9	20.9	19.9	20.4	18.5	20.4	19.9	23.4	22.5	20.9	19.3	19.3	21.3	17.1	16.1		24.5	22.1	24.4
MN031239_NewtDV	21.8	20.6	19.7	20.6	18.9	19	20.2	20.2	19.6	18.8	20.1	16.9	17.3	17.8	16.7	21.1	14.7		22.9	24.3
MK962760_ToadDV	20.7	24.6	20.9	20.9	20.4	21	19.3	19.9	18.2	20.4	20.9	20.2	20.2	18.6	18.4	20.1	16.8	16.2		19.8
MK962759_TermiteDV	20	18.2	20.1	21.6	19.7	22.2	21.1	21.1	20.1	19.7	21.6	19	21	20.5	18.8	21.5	10.8	14.9	10.4	

Fig. S1. Genetic distances matrices showing representative deltavirus sequences with percent nucleotide identities between genomes (upper triangle) and percent amino acid identities between complete DAg sequences (lower triangle). Darker shading indicates higher percentage identity between two deltaviruses

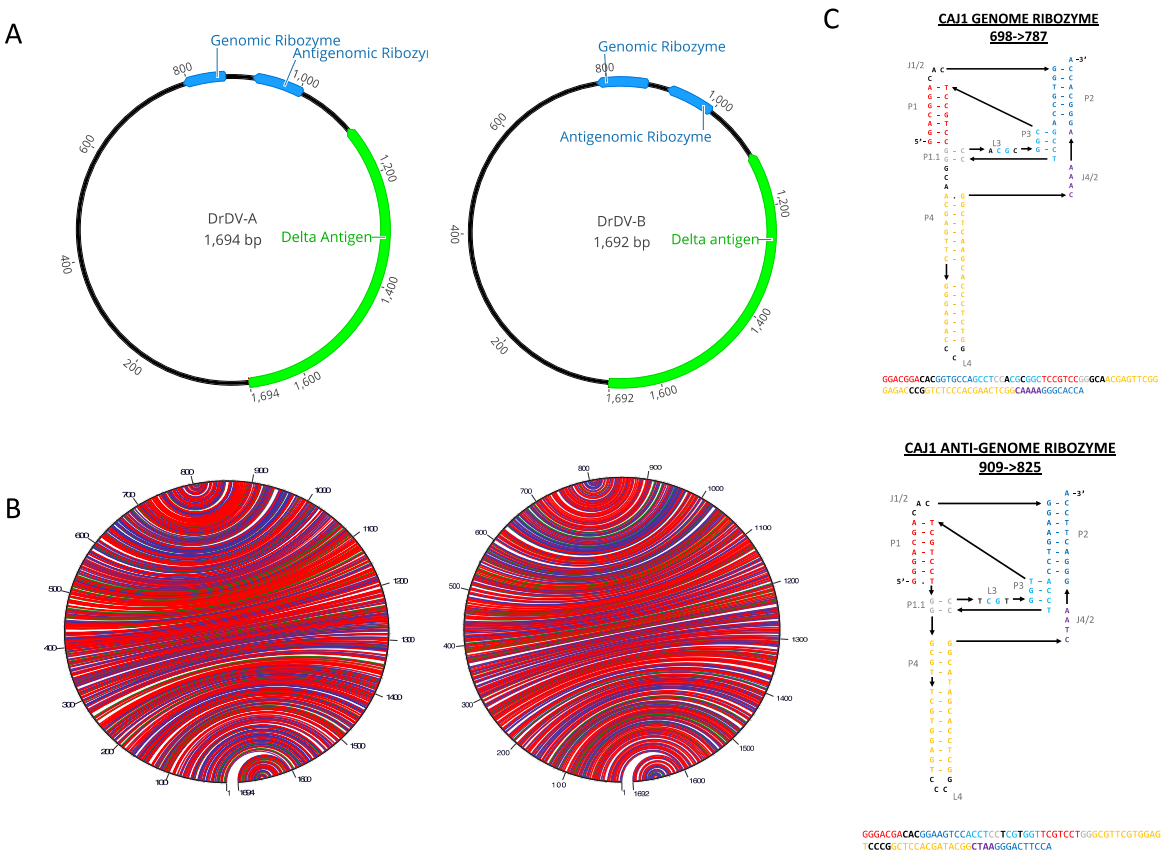

796

797 **Fig. S2. DrDV genomes exhibit characteristics common to deltaviruses.** (A) The locations of
798 the delta antigen open reading frame (green) and genomic/antigenomic ribozymes (blue) are
799 shown along the circular genomes of DrDV-A and DrDV-B (CAJ1 shown as an example). (B)
800 Intramolecular base pairing for DrDVs depicted as lines connecting points on the circular genome
801 – G-C pairs are red, A-U pairs are blue, G-U pairs are green, other pairs are yellow. (C) Genomic
802 and antigenomic ribozyme secondary structures are shown along with genome location for genome
803 CAJ1. Complementary regions are shown in the same color, and structures are depicted in the style
804 of Webb & Luptak to facilitate comparison with ribozymes from previous studies (*9*, *10*, *45*)**.**

805

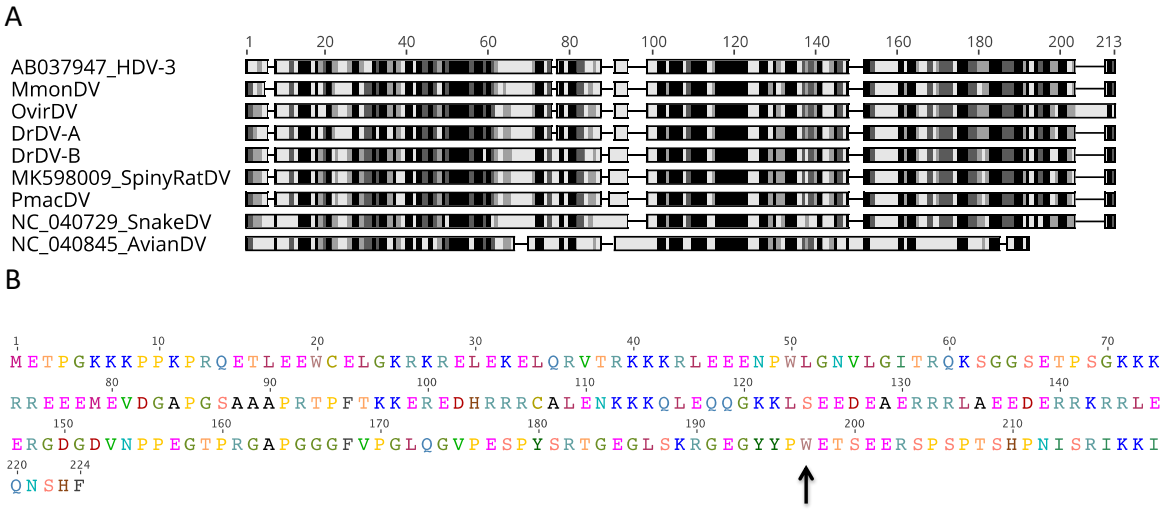

806

807 **Fig. S3. Characterization of DrDV delta antigen proteins.** (A) Alignment of delta antigen
808 protein sequences for mammalian, snake and avian deltaviruses. Shading indicates level of
809 similarity across all sequences, with regions of highest identity in black. (B) Putative sequence of
810 the large DAg for the DrDV-B virus from the site CAJ1. The RNA editing site is marked with a
811 black arrow; UAG has been edited to UGG yielding a tryptophan residue (W).

812

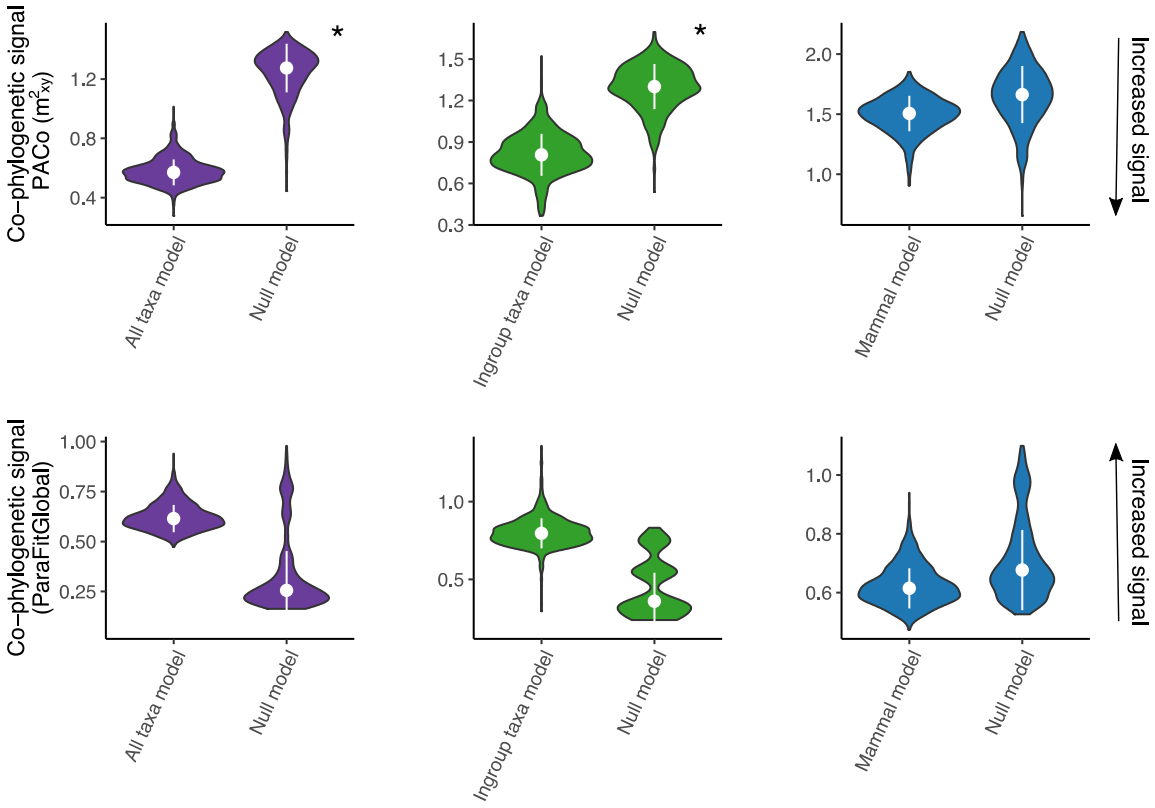

813 **Fig. S4. Co-phylogenetic signal in subsets of the deltavirus phylogeny.** Violin plots show the
814 degree of dependence of 1,000 phylogenies from the posterior of the StarBeast analysis (Fig. S5)
815 on the host phylogeny relative to null models, with the median and standard deviation. Data subsets
816 are colored as in Fig. 2B (All taxa: purple+green+blue, Ingroup: green+blue, mammals: blue)
817 Distributions are shown for analyses performed using PACo (top row) and ParaFit (bottom row).
818 Asterisks show significant dependence of the virus phylogeny on the host phylogeny ($P < 0.05$).
819 Note that lower values of the empirical model relative to the null model represent increased signal
820 of co-phylogeny in PACo while higher values represent increased signal of co-phylogeny in
821 ParaFit.

822

823

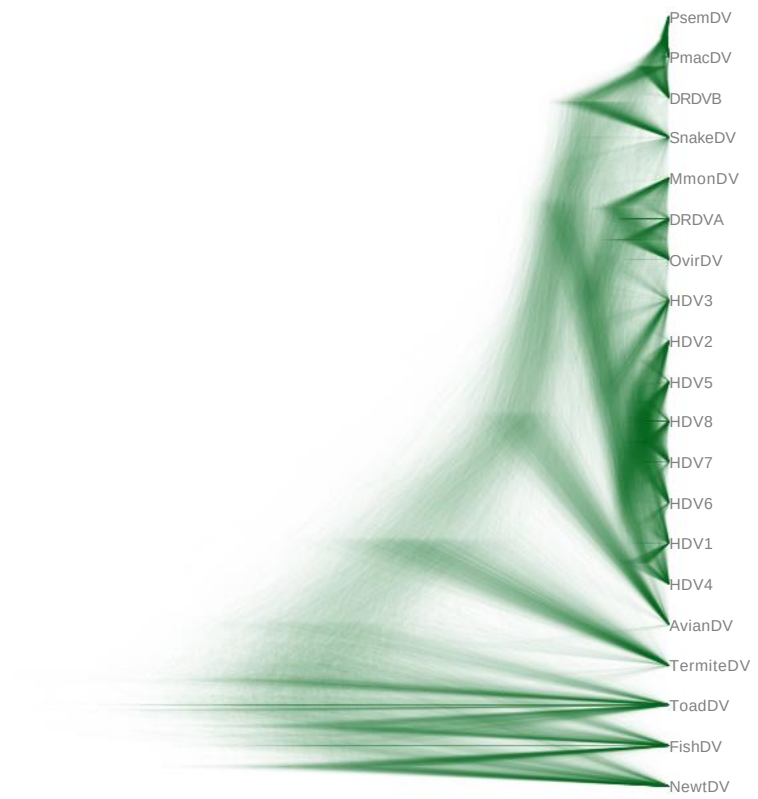

824

825 **Fig. S5. Uncertainty of deep relationships in the deltavirus phylogeny.** The DensiTree shows
826 the distribution of 1,000 posterior trees from the StarBeast analysis, highlighting uncertainties in
827 the evolutionary relationships among divergent deltavirus-like taxa.

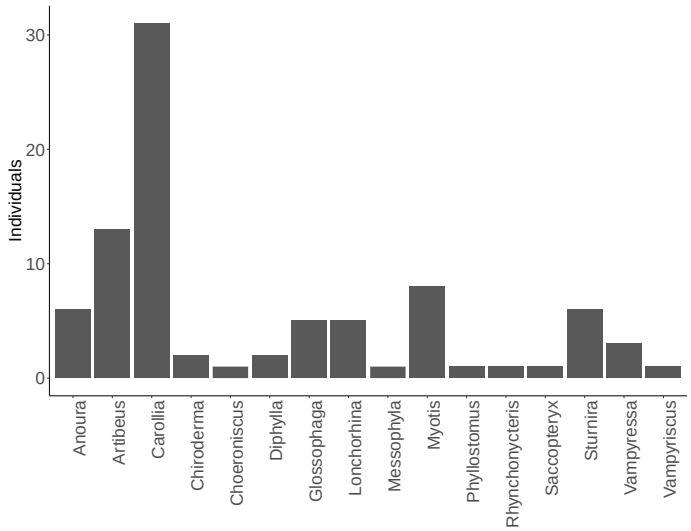

Fig. S6. Counts of non-*D. rotundus* bat species saliva swabs individually screened by RT-PCR for DrDV-B. Bars group bats by genus.

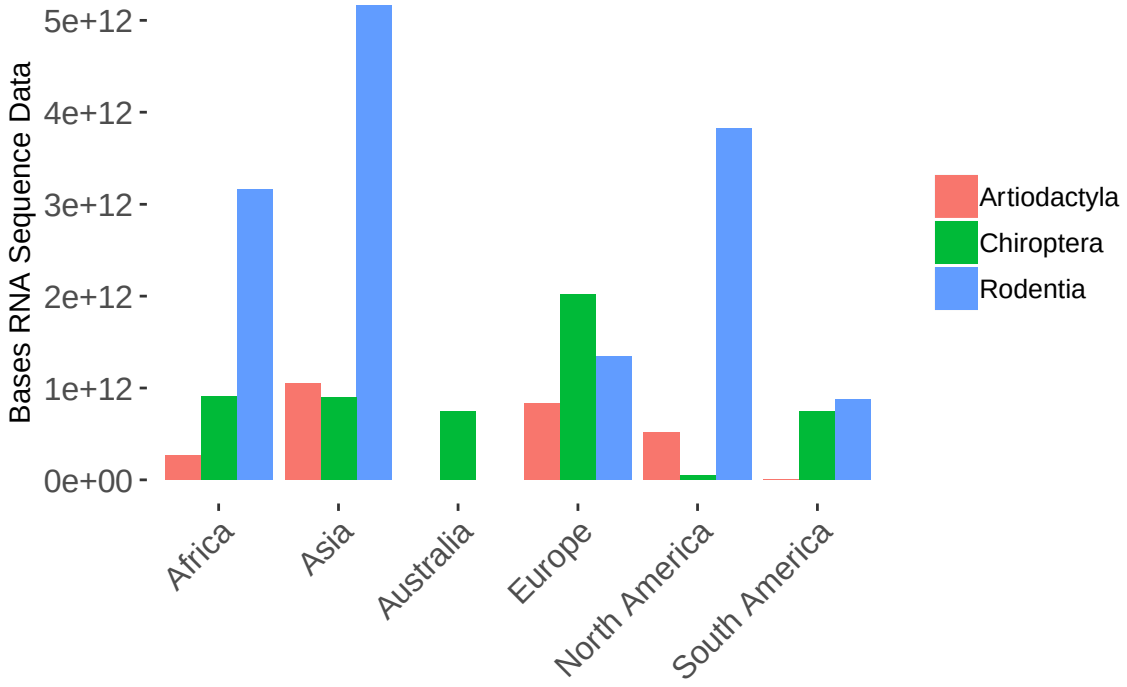

833

834 **Fig S7. Continent level geographic biases in RNA sequence data examined by Serratus.** Bars
835 are colored by mammalian order; data shown are limited to the three orders in which deltaviruses
836 were detected.

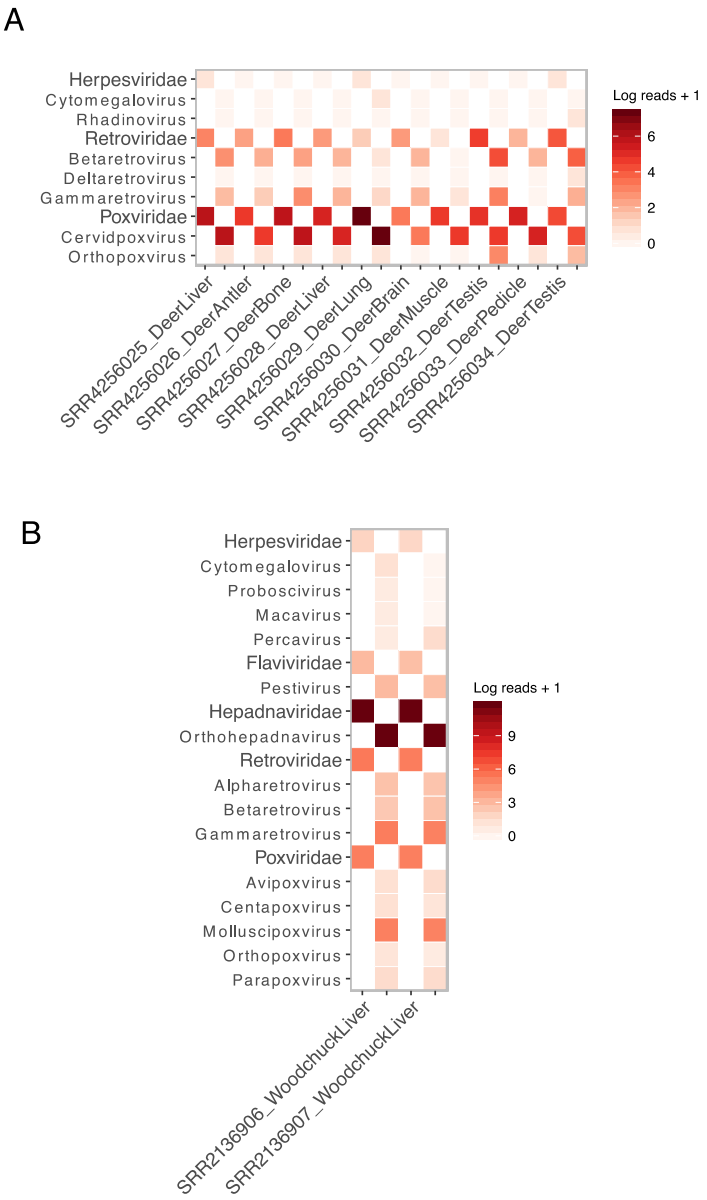

837

838 **Fig S8. Candidate helper viruses for the OvirDV and MmonDV datasets.** Mammal-infecting
839 viral communities are shown for (A) *O. virginianus* libraries sequenced by RNASeq from (*17*),
840 several of which contained OvirDV and (B) two *M. monax* samples infected with MmonDV from
841 (*18*). Viral families (in larger font) and genera are shown in adjacent columns for each sample,
842 with families on the left and genera on the right.

843

844

Supplementary Tables

Table S1. Pooled bat saliva samples from Peru analyzed by metagenomic sequencing.

Genus	Species	Individuals in pool	Raw reads	Deltavirus contig length (bp)
Carollia	*perspicillata*	10*	28,700,978	N
Glossophaga	*soricina*	5	24,079,752	N
Desmodus	*rotundus*	10	28,946,275	921†
Diphylla	*ecaudata*	2	25,023,095	N
Anoura	*geoffroyi peruana*	6	18,569,505	N
Artibeus	*lituratus obscurus planirostris fraterculus*	10	14,966,399	N
Myotis	*oxyotus unidentified sp*	8	19,934,479	N
Sturnira	*erythromos unidentified sp*	6	11,348,995	N
Vampyressa/ Vampyriscus	*bidens unidentified sp*	4	13,734,389	N
Rare species	*Chiroderma trinitatum Chiroderma salvini Choeroniscus minor Rhynchonycteris naso Saccopteryx bilineata Messophyla macconelli Phyllostomus discolor Rhinophylla pumilio*	8	16,746,795	N

*Pool included individual CP-1 in which DrDV-B was detected by RT-PCR

†Pool was identical to CAJ1 pool where DrDV was initially discovered, confirming the ability to detect deltaviruses when they are known to be present

851 **Table S2. Deltavirus positive cohorts evaluated by mapping reads from related libraries to**
852 **novel deltavirus genomes.**

SRA accession	Pool ID	Host§	DV Reads¶
ERR2756783	AAC_H_F	*Desmodus rotundus*	2 (DrDV-A)
ERR2756784	AAC_H_SV*	*Desmodus rotundus*	189 (DrDV-A) 18 (DrDV-B)
ERR2756785	AAC_L_F	*Desmodus rotundus*	0
ERR2756786	AAC_L_SV	*Desmodus rotundus*	0
ERR2756787	AMA_L_ F_NR	*Desmodus rotundus*	0
ERR2756788	AMA_L_F_R	*Desmodus rotundus*	0
ERR2756789	AMA_L_SV	*Desmodus rotundus*	0
ERR2756790	CAJ_L_F_NR	*Desmodus rotundus*	0
ERR2756791	CAJ_L_F_R	*Desmodus rotundus*	0
ERR2756792	CAJ_L_SV	*Desmodus rotundus*	4
ERR2756793	CAJ_H_F_1	*Desmodus rotundus*	0
ERR2756794	CAJ_H_F_2	*Desmodus rotundus*	4
ERR2756795	CAJ_H_SV*	*Desmodus rotundus*	169
ERR2756796	HUA_H_F	*Desmodus rotundus*	2
ERR2756797	HUA_H_SV	*Desmodus rotundus*	0
ERR2756798	LMA_L_F_NR	*Desmodus rotundus*	0
ERR2756799	LMA_L_F_R	*Desmodus rotundus*	0
ERR2756800	LMA_L_SV_NR	*Desmodus rotundus*	45
ERR2756801	LMA_L_SV_R*	*Desmodus rotundus*	320
ERR2756802	LR_L_F_NR	*Desmodus rotundus*	0
ERR2756803	LR_L_F_R	*Desmodus rotundus*	0
ERR2756804	LR_L_SV	*Desmodus rotundus*	0
ERR3569452	AMA2_H	*Desmodus rotundus*	0
ERR3569453	AMA2_SV	*Desmodus rotundus*	0
ERR3569454	API1_H	*Desmodus rotundus*	0
ERR3569455	API1_SV	*Desmodus rotundus*	0
ERR3569456	API17_H	*Desmodus rotundus*	0
ERR3569457	API17_SV	*Desmodus rotundus*	2 (DrDV-A)
ERR3569458	API140_H	*Desmodus rotundus*	32

ERR3569459	API140_SV	*Desmodus rotundus*	0
ERR3569460	API141_H	*Desmodus rotundus*	0
ERR3569461	API141_SV	*Desmodus rotundus*	0
ERR3569462	AYA1_H	*Desmodus rotundus*	2
ERR3569463	AYA1_SV	*Desmodus rotundus*	0
ERR3569464	AYA7_H	*Desmodus rotundus*	0
ERR3569465	AYA7_SV	*Desmodus rotundus*	18
ERR3569466	AYA11_H	*Desmodus rotundus*	0
ERR3569467	AYA11_SV*	*Desmodus rotundus*	591
ERR3569468	AYA12_H	*Desmodus rotundus*	0
ERR3569469	AYA12_SV	*Desmodus rotundus*	2
ERR3569470	AYA14_H	*Desmodus rotundus*	0
ERR3569471	AYA14_SV*	*Desmodus rotundus*	228 (DrDV-A) 2 (DrDV-B)
ERR3569472	AYA15_H	*Desmodus rotundus*	0
ERR3569473	AYA15_SV	*Desmodus rotundus*	0
ERR3569474	CAJ1_H	*Desmodus rotundus*	0
ERR3569475	CAJ1_SV*	*Desmodus rotundus*	172
ERR3569476	CAJ2_H	*Desmodus rotundus*	4
ERR3569477	CAJ2_SV†	*Desmodus rotundus*	0
ERR3569478	CAJ4_H	*Desmodus rotundus*	0
ERR3569479	CAJ4_SV†	*Desmodus rotundus*	0
ERR3569480	CUS8_H	*Desmodus rotundus*	0
ERR3569481	CUS8_SV	*Desmodus rotundus*	4
ERR3569482	HUA1_H	*Desmodus rotundus*	0
ERR3569483	HUA1_SV	*Desmodus rotundus*	0
ERR3569484	HUA2_H	*Desmodus rotundus*	5
ERR3569485	HUA2_SV	*Desmodus rotundus*	0
ERR3569486	HUA3_H	*Desmodus rotundus*	0
ERR3569487	HUA3_SV	*Desmodus rotundus*	0
ERR3569488	HUA4_H	*Desmodus rotundus*	0
ERR3569489	HUA4_SV	*Desmodus rotundus*	0
ERR3569490	LMA5_H	*Desmodus rotundus*	0
ERR3569491	LMA5_SV	*Desmodus rotundus*	8

ERR3569492	LMA6_H	*Desmodus rotundus*	0
ERR3569493	LMA6_SV*	*Desmodus rotundus*	173
ERR3569494	LR2_H	*Desmodus rotundus*	0
ERR3569495	LR2_SV	*Desmodus rotundus*	0
ERR3569496	LR3_H	*Desmodus rotundus*	0
ERR3569497	LR3_SV	*Desmodus rotundus*	0
SRR7910142	Pm_03	*Peropteryx macrotis*	0
SRR7910143	Pm_01*	*Peropteryx macrotis*	346
SRR7910144	Pm_02	*Peropteryx macrotis*	2
SRR7910145	Nl_02‡	*Nyctinomops laticaudatus*	0
SRR7910146	Nl_03‡	*Nyctinomops laticaudatus*	0
SRR7910147	Mk_01‡	*Myotis keaysi*	0
SRR7910148	Mk_02‡	*Myotis keaysi*	0
SRR7910149	Mm_02‡	*Mormoops megalophylla*	0
SRR7910150	Mm_03‡	*Mormoops megalophylla*	0
SRR7910151	Aj_03‡	*Artibeus jamaicensis*	0
SRR7910152	Mm_01‡	*Mormoops megalophylla*	0
SRR7910153	Aj_01‡	*Artibeus jamaicensis*	0
SRR7910154	Aj_02‡	*Artibeus jamaicensis*	0
SRR7910155	Mk_03‡	*Myotis keaysi*	0
SRR7910156	Nl_01‡	*Nyctinomops laticaudatus*	0
SRR4256025	Deer-Liver-1-male	*Odocoileus virginianus*	0
SRR4256026	Deer-Antler-2-male	*Odocoileus virginianus*	12
SRR4256027	Deer-Bone-1-male	*Odocoileus virginianus*	0
SRR4256028	Deer-Liver-2-male	*Odocoileus virginianus*	0
SRR4256029	Deer-Lung-1-male	*Odocoileus virginianus*	0
SRR4256030	Deer-Brain-2-male	*Odocoileus virginianus*	12
SRR4256031	Deer-Muscle-2-male	*Odocoileus virginianus*	14
SRR4256032	Deer-Testis-1-male	*Odocoileus virginianus*	0
SRR4256033	Deer-Pedicle-male*	*Odocoileus virginianus*	9265
SRR4256034	Deer-Testis-2-male	*Odocoileus virginianus*	7

853

854 * Pools in which full deltavirus genomes were detected

855 † Pools in which DrDV was detected in the saliva of one or more individuals in the pool by RT-PCR, but
856 were negative for deltavirus detection through metagenomics
857 ‡Species in which deltaviruses were not detected but which came from the same study
858 §*D. rotundus* samples represent saliva (SV) and fecal (F/H) samples pooled across multiple individuals
859 from different sites. Samples from other Neotropical bats (*P. macrotis, N. laticaudatus, M. keaysi, M.*
860 *megalophylla, A. jamaicensis*) represent liver samples from unique individuals. *O. virginianus* samples
861 represent different tissues pooled across multiple individuals. Read mapping of samples from different
862 individuals and time points to the MmonDV genome is described in (*1*)
863 ¶Samples from *D. rotundus* were mapped to DrDV-A and DrDV-B genomes. All *D. rotundus* read counts
864 refer to DrDV-B genomes unless specifically noted as DrDV-A. In the case of libraries with matches to
865 both, the number of reads mapping is broken down by DrDV-genome. Samples from *P. macrotis, N.*
866 *laticaudatus, M. keaysi, M. megalophylla, A. jamaicensis* were mapped to the PmacDV genome. Samples
867 from *O. virginianus* were mapped to OvirDV.
868

869 **Table S3. Summary statistics for bat deltavirus genomes and protein domain homology**
870 **analysis of predicted DrDV small delta antigens from saliva metagenomic pools.**

871

Site	Lineage	Genome (nt)	GC content (%)	Intramolecular base pairing (%)	Delta antigen (aa)	Hhpred top hit	Probability top hit	e-value	Identity top hit (%)	Genbank accession
AYA14	DrDV-A	1694	55	73.8	194	Oligomerization	99.86	2.8e-25	59	MT649207
AYA11	DrDV-B	1692	54.3	75.3	196	domain of	99.86	5.60E-25	45	MT649206
CAJ1	DrDV-B	1692	53.8	74.3	196	hepatitis delta	99.86	5.40E-25	45	MT649208
LMA6	DrDV-B	1694	54.3	74.6	196	antigen	99.85	8.30E-25	45	MT649209

872

873

874 **Table S4. Primers used to screen samples for DrDV by RT-PCR and HBV by PCR.**

875

Primer	PCR Round	Sequence (5´-3´)
DrDV-A		
DrDV_F1_GenoA	1&2	AGGGGTCTTTTTGGGAAATT
DrDV_R1_GenoA	1	AAGAAGAAGCAACTATCCGG
DrDV_R2_GenoA	2	CATCCAAGAGACCAAGAGAG
DrDV-B		
DrDV_F1_GenoB	1	TTCCCTTGYTGCTCCAGTTG
DrDV_R1_GenoB	1	CGGTAAGAAGAAACCTCCAA
DrDV_F2_GenoB	2	CCAGTTGTTTCTTCTTGTTCTC
DrDV_R2_GenoB	2	AAAAAGAAAGAGAGAACTGGAAAAA
DrDV Delta Antigen		
DeltaAntigenF1_GenoB	1	TCTGGTCTTATCTTTCTTACCTTAT
DeltaAntigenR1_GenoB	1	AAACCTTCCTTTATTCTATTTCGAA
DeltaAntigenR1_GenoA	1	CCTTTACCTTTAATTCTCTTGGTAA
DeltaAntigenF1_GenoA	1	GCCTCGAATAATAAGAAGAAAATTT
HBV Primers*		
HBV-F248	1&2	CTAGATTBGTGGTGGACTTCTCTCA
HBV-R397	2	GATARAACGCCGCAGATACATCCA
HBV-R450a	1	TCCAGGAGAACCAAYAAGAAAGTGA
HBV-R450b	1	TCCAGGAGAACCAAYAAGAAGATGA

876

877 *Primer sequences and PCR protocol described in (*38*)

878

879

880

881 **Table S5. Colony level demographic characteristics and PCR-based screening results of**
882 **vampire bat blood and saliva for DrDV and HBV.**

883

			DrDV-A		DrDV-B		HBV	
Colony	Prop Male*	Prop Adult†	Saliva	Blood	Saliva	Blood	Saliva	Blood
AYA1	0.6	1	0/20	0/20	3/20	0	0/3	0/20
AYA11	0.6	0.95	0/20	0/20	2/20	0	0/3	0/20
AYA14	0.4	0.65	1/20	0/20	4/20	0	0/8	0/20
AYA15	0.55	0.75	0/20	0	0/20	0	0	0
CAJ1	0.75	0.9	0/20	0	5/20	0/20	0/10	0/20
CAJ2	0.55	0.95	0/20	0	6/20	6/20	0/6	0/20
CAJ3	0.7	1	0/20	0	4/20	0	0/4	0
CAJ4	0.35	0.75	0/20	0	2/20	0	0/2	0
LMA4	0.65	0.75	0/20	0	0/20	0	0/1	0
LMA5	0.65	0.9	0/20	0	5/20	0	0/5	0
LMA6	0.35	1	0/20	0	7/20	4/20	0/9	0/19
LMA12	0.5	0.9	0/20	0	3/20	0	0/3	0
Total	-	-	1/240	0/60	41/240	10/60	0/54	0/119

884

885 *Proportion of males at each colony (alternative is females)

886 †Proportion of adults at each colony (alternatives are juveniles or subadults)

887

888 **Table S6. Test of association between DrDV-B phylogeny and sample location at the**
889 **regional (department) and colony level.**

890

Level	Index	Observed value (95% CI)	Null value (95% CI)	p-value
Region	AI*	0.22 (0-0.58)	2.46 (1.95-2.94)	0
	PS†	4 (3-5)	17.73 (15.41-19.35)	0
	MC‡ (LMA)	9.29 (5-14)	1.97 (1.41-2.98)	0.001
	MC‡ (CAJ)	11.24 (9-19)	2.81 (2.12-3.94)	0.001
	MC‡ (AYA)	2.67 (1-5)	1.26 (1-1.96)	0.02
Colony	AI*	2.23 (1.69-2.76)	3.63 (3.21-3.92)	0
	PS†	19.19 (18-20)	29.23 (27.45-30.81)	0
	MC‡ (LMA6)	4.98 (5-5)	1.18 (1-1.94)	0.001
	MC‡ (LMA5)	2.52 (1-3)	1.13 (1-1.43)	0.002
	MC‡ (CAJ2)	3.21 (2-6)	1.57 (1.14-2.39)	0.01
	MC‡ (CAJ1)	1 (1-1)	1.13 (1-1.53)	1
	MC‡ (AYA1)	1.09 (1-2)	1.01 (1-1.05)	1
	MC‡ (CAJ3)	1.01 (1-1)	1.07 (1-1.32)	1
	MC‡ (AYA11)	1.03 (1-1)	1.01 (1-1.05)	1
	MC‡ (AYA14)	1.05 (1-2)	1.04 (1-1.15)	1
	MC‡ (CAJ4)	1.16 (1-2)	1.01 (1-1.05)	1
	MC‡ (LMA12)	1 (1-1)	1.04 (1-1.15)	1

891

892 *Association Index

893 † Parsimony Score

894 ‡ Monophyletic Clade size

895

Supplementary References

1. R. C. Edgar *et al.*, Petabase-scale sequence alignment catalyses viral discovery. *bioRxiv*, 1–30 (2020).

2. L. M. Bergner *et al.*, Using noninvasive metagenomics to characterize viral communities from wildlife. *Mol Ecol Resour*. **19**, 128–143 (2019).

3. L. M. Bergner *et al.*, Demographic and environmental drivers of metagenomic viral diversity in vampire bats. *Mol Ecol*. **29**, 26–39 (2020).

4. A. Bankevich *et al.*, SPAdes: A New Genome Assembly Algorithm and Its Applications to Single-Cell Sequencing. *J Comput Biol*. **19**, 455–477 (2012).

5. M. Kearse *et al.*, Geneious Basic: An integrated and extendable desktop software platform for the organization and analysis of sequence data. *Bioinformatics*. **28**, 1647–1649 (2012).

6. P. Rice, I. Longden, A. Bleasby, EMBOSS: The European molecular biology open software suite. *Trends Genet*. **16**, 276–277 (2000).

7. K. Katoh, K. Misawa, K.-I. Kuma, T. Miyata, MAFFT: a novel method for rapid multiple sequence alignment based on fast Fourier transform. *Nucleic Acids Res*. **30**, 3059–3066 (2002).

8. J. Söding, A. Biegert, A. N. Lupas, The HHpred interactive server for protein homology detection and structure prediction. *Nucleic Acids Res*. **33**, W244–W248 (2005).

9. M. Wille *et al.*, A Divergent Hepatitis D-Like Agent in Birds. *Viruses*. **10**, 720–9 (2018).

10. U. Hetzel *et al.*, Identification of a Novel Deltavirus in Boa Constrictors. *mBio*. **10**, 1447–8 (2019).

11. M. Zuker, Mfold web server for nucleic acid folding and hybridization prediction. *Nucleic Acids Res*. **31**, 3406–3415 (2003).

12. S. Bellaousov, J. S. Reuter, M. G. Seetin, D. H. Mathews, RNAstructure: Web servers for RNA secondary structure prediction and analysis. *Nucleic Acids Res*. **41**, W471–W474 (2013).

13. S. L. Kosakovsky Pond, D. Posada, M. B. Gravenor, C. H. Woelk, S. D. W. Frost, GARD: a genetic algorithm for recombination detection. *Bioinformatics*. **22**, 3096–3098 (2006).

14. S. Weaver *et al.*, Datamonkey 2.0: A Modern Web Application for Characterizing Selective and Other Evolutionary Processes. *Mol Biol Evol*. **35**, 773–777 (2018).

15. H. Li, R. Durbin, Fast and accurate short read alignment with Burrows-Wheeler transform. *Bioinformatics*. **25**, 1754–1760 (2009).

16. D. D. Moreno-Santillán, C. Machain-Williams, G. Hernández-Montes, J. Ortega, De Novo Transcriptome Assembly and Functional Annotation in Five Species of Bats. *Sci Rep.* **9**, 6222–12 (2019).

17. C. M. Seabury *et al.*, Genome-Wide Polymorphism and Comparative Analyses in the White-Tailed Deer (Odocoileus virginianus): A Model for Conservation Genomics. *PLOS ONE*. **6**, e15811–9 (2011).

18. S. P. Fletcher *et al.*, Intrahepatic Transcriptional Signature Associated with Response to Interferon-α Treatment in the Woodchuck Model of Chronic Hepatitis B. *PLoS Pathog*. **11**, e1005103–30 (2015).

19. R Core Team, R: A language and environment for statistical computing. R Foundation for Statistical Computing. (available at www.r-project.org) (2019).

20. K. E. Jones *et al.*, PanTHERIA: a species-level database of life history, ecology, and geography of extant and recently extinct mammals. *Ecology*. **90**, 2648–2648 (2009).

21. S. Kalyaanamoorthy, B. Q. Minh, T. K. F. Wong, A. von Haeseler, L. S. Jermiin, ModelFinder: fast model selection for accurate phylogenetic estimates. *Nat Meth*. **14**, 587–589 (2017).

22. B. Q. Minh *et al.*, IQ-TREE 2: New Models and Efficient Methods for Phylogenetic Inference in the Genomic Era. *Mol Biol Evol*. **37**, 1530–1534 (2020).

23. A. J. Drummond, M. A. Suchard, D. Xie, A. Rambaut, Bayesian phylogenetics with BEAUti and the BEAST 1.7. *Mol Biol Evol*. **29**, 1969–1973 (2012).

24. J. A. Balbuena, R. Míguez-Lozano, I. Blasco-Costa, PACo: A Novel Procrustes Application to Cophylogenetic Analysis. *PLOS ONE*. **8**, e61048 (2013).

25. M. C. Hutchinson, E. F. Cagua, J. A. Balbuena, D. B. Stouffer, T. Poisot, paco: implementing Procrustean Approach to Cophylogeny in R. *Methods Ecol Evol*. **8**, 932–940 (2017).

26. P. Legendre, Y. Desdevises, E. Bazin, A Statistical Test for Host–Parasite Coevolution. *Syst Biol*. **51**, 217–234 (2002).

27. E. Paradis, K. Schliep, ape 5.0: an environment for modern phylogenetics and evolutionary analyses in R. *Bioinformatics*. **35**, 526–528 (2019).

28. K. P. Schliep, phangorn: phylogenetic analysis in R. *Bioinformatics*. **27**, 592–593 (2010).

29. L. J. Revell, phytools: an R package for phylogenetic comparative biology (and other things). *Methods Ecol Evol*. **3**, 217–223 (2011).

30. G. Yu, D. K. Smith, H. Zhu, Y. Guan, T. T.-Y. Lam, ggtree: an rpackage for visualization and annotation of phylogenetic trees with their covariates and other associated data. *Methods Ecol Evol*. **8**, 28–36 (2016).

31. F. M. Martins, A. D. Ditchfield, D. Meyer, J. S. Morgante, Mitochondrial DNA phylogeography reveals marked population structure in the common vampire bat, Desmodus rotundus (Phyllostomidae). *J Zool Syst Evol Res*. **45**, 372–378 (2007).

32. S. Capella-Gutiérrez, J. M. Silla-Martínez, T. Gabaldón, trimAl: a tool for automated alignment trimming in large-scale phylogenetic analyses. *Bioinformatics*. **25**, 1972–1973 (2009).

33. D. Darriba, G. L. Taboada, R. Doallo, D. Posada, jModelTest 2: more models, new heuristics and parallel computing. *Nat Meth*. **9**, 772–772 (2012).

34. F. Ronquist *et al.*, MrBayes 3.2: efficient Bayesian phylogenetic inference and model choice across a large model space. *Syst Biol*. **61**, 539–542 (2012).

35. J. Parker, A. Rambaut, O. G. Pybus, Correlating viral phenotypes with phylogeny: Accounting for phylogenetic uncertainty. *Infect Genet Evol*. **8**, 239–246 (2008).

36. D. Bates, M. Mächler, Bolker, S. Walker, Fitting Linear Mixed-Effects Models Using lme4. *J. Stat Softw*. **67** (2015), doi:10.18637/jss.v067.i01.

37. J. Fox, S. Weisberg, *An R Companion to Applied Regression* (Sage, Thousand Oaks, CA, Second Edition. 2011).

38. J. F. Drexler *et al.*, Bats carry pathogenic hepadnaviruses antigenically related to hepatitis B virus and capable of infecting human hepatocytes. *Proc Natl Acad Sci USA.* **110**, 16151–16156 (2013).

39. B. Buchfink, C. Xie, D. H. Huson, Fast and sensitive protein alignment using DIAMOND. *Nat Meth*. **12**, 59–60 (2014).

40. K. D. Pruitt, T. Tatusova, D. R. Maglott, NCBI reference sequences (RefSeq): a curated non-redundant sequence database of genomes, transcripts and proteins. *Nucleic Acids Res*. **35**, D61–D65 (2007).

41. B. D. Ondov, N. H. Bergman, A. M. Phillippy, Interactive metagenomic visualization in a Web browser. *BMC Bioinformatics*, 385 (2011).

42. D. H. Huson *et al.*, MEGAN Community Edition - Interactive Exploration and Analysis of Large-Scale Microbiome Sequencing Data. *PLoS Comput Biol*. **12**, e1004957–12 (2016).

43. J. L. Casey, K. F. Bergmann, T. L. Brown, J. L. Gerin, Structural requirements for RNA editing in hepatitis delta virus: evidence for a uridine-to-cytidine editing mechanism. *Proc Natl Acad Sci USA.* **89**, 7149–7153 (1992).

995 44. S. B. Hwang, M. Lai, Isoprenylation Mediates Direct Protein-Protein Interactions
996 Between Hepatitis Large Delta-Antigen and Hepatitis-B Virus Surface-Antigen. *J Virol*.
997 **67**, 7659–7662 (1993).

998 45. C.-H. T. Webb, A. Lupták, HDV-like self-cleaving ribozymes. *RNA Biol*. **8**, 719–727
999 (2014).